DIODE-LASER-PUMPED OPTICAL PARAMETRIC OSCILLATOR

Marc C. Cimolino et al.

Cygnus Laser Corporation
P.O. Box 1730
Duvall, WA 98019-1730

October 1996

Final Report

APPROVED FOR PUBLIC RELEASE; DISTRIBUTION IS UNLIMITED.

PHILLIPS LABORATORY
Lasers and Imaging Directorate
AIR FORCE MATERIEL COMMAND
KIRTLAND AIR FORCE BASE, NM 87117-5776

19970509 061

DTIC QUALITY INSPECTED 1

PL-TR-96-1105

Using Government drawings, specifications, or other data included in this document for any purpose other than Government procurement does not in any way obligate the U.S. Government. The fact that the Government formulated or supplied the drawings, specifications, or other data, does not license the holder or any other person or corporation; or convey any rights or permission to manufacture, use, or sell any patented invention that may relate to them.

This report has been reviewed by the Public Affairs Office and is releasable to the National Technical Information Service (NTIS). At NTIS, it will be available to the general public, including foreign nationals.
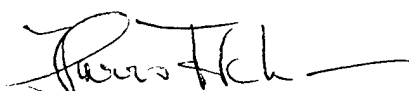
If you change your address, wish to be removed from this mailing list, or your organization no longer employs the addressee, please notify PL/LIDD, 3550 Aberdeen Ave SE, Kirtland AFB, NM 87117-5776.

Do not return copies of this report unless contractual obligations or notice on a specific document requires its return.

This report has been approved for publication.

KENNETH D. SHAW
Project Manager

FOR THE COMMANDER

HARRO ACKERMANN, GS-13
Branch Chief, PL/LIDD

ROBERT A. DURYEA, Colonel, USAF
Director, Lasers and Imaging Directorate

1. Report Date (dd-mm-yy) October 96	2. Report Type Final	3. Dates covered (from... to) Aug '94 - Oct '96	
4. Title & subtitle Diode-Laser-Pumped Optical Parametric Oscillator		5a. Contract or Grant # F29601-94-C-0144	
		5b. Program Element # 65502F	
6. Author(s) Marc C. Cimolino, Carrie Sjaarda-Cornish, Robert Byer, Martin M. Fejer, Robert C. Eckardt, Lawrence E. Myers, Robert Batchko		5c. Project # 3005	
		5d. Task # CO	
		5e. Work Unit # CJ	
7. Performing Organization Name & Address Cygnus Laser Corporation P.O. Box 1730 Duvall, WA 98019-1730		8. Performing Organization Report #	
9. Sponsoring/Monitoring Agency Name & Address Phillips Laboratory 3550 Aberdeen Ave SE Kirtland AFB, NM 87117-5776		10. Monitor Acronym PL/LIDA	
		11. Monitor Report # PL-TR-96-1105	

13. Supplementary Notes

14. Abstract
This report describes the first operation of a CW directly diode-pumped optical parametric oscillator using periodically poled lithium niobate as a nonlinear medium. Degenerate oscillation of a doubly resonant device was sucessful. This device shows potential as a CW source in the near infrared region from 1.3 - 5 microns.

15. Subject Terms
Optical Parametric Oscillator, Laser, PPLN, Lithium Niobate

Security Classification of			19. Limitation of Abstract	20. # of Pages	21. Responsible Person (Name and Telephone #)
16. Report Unclassified	17. Abstract Unclassified	18. This Page Unclassified	Unlimited	82	Kenneth Shaw (505)846-5941

Contents

List of Figures

1 PROJECT SUMMARY

1.1 Purpose of Research

The purpose of our Phase II technical program was to build and deliver a continuous wave (CW), diode-pumped optical parametric oscillator (OPO). This required the advancement of state-of-the-art technology in three important areas, previously identified in our Phase I work. The first item was to improve performance of the Master Oscillator-Power Amplifier (MOPA) diodes that are used as the pump source for the OPO. The second item was to improve the engineering of the periodically poled lithium niobate (PPLN)—the nonlinear crystal used for parametric oscillation—to increase efficiency and reduce threshold. The third item to be addressed was the development of trichroic coatings that exhibited the necessary reflectivities for specific wavelengths. These advancements were to be incorporated into a deliverable unit to Phillips Laboratory.

1.2 Research Description

A CW diode-pumped OPO was assembled. The PPLN fabrication process was refined and suitable pieces were obtained from Stanford University for use as the parametric oscillator crystal in the OPO. The OPO resonator was a near spherical doubly resonant configuration that had a degenerate mode of operation. The cavity was pumped by a MOPA laser diode, and the coatings on the PPLN were fabricated by Lightning Optical. A rigorous model of OPO operation was developed for PPLN. Degenerate operation was successfully acheived. Nondegenerate operation was not acheived due to pump laser instabilities, nor was the high power pumping experiment performed.

1.3 Research Results

We achieved parametric oscillation for short periods of time using the MOPA diode laser from SDL. The performance of the OPO when pumped with two different sources was distinctly different and demonstrated the versatility of a diode-pumped OPO. The experiments performed using the broader linewidth MOPA resulted in an output that could be scanned over a 200 nm range in 1 millisecond—a result of the cluster effect[5]. When we used the narrow linewidth MOPA, the cluster effect did not occur and a stable output at a single frequency was observed. Each of these effects is an important feature of a mid-infrared source designed for the applications listed below.

1.4 Potential Applications

Applications for tunable laser light from 1.3 to 5 μm include communications, analytical chemistry, infrared optical counter measures, the detection and spectroscopy of trace compounds found in the atmosphere, and laser propagation through specific transparent regions in the atmosphere. A tunable source that can operate efficiently over a wide wavelength range and that is compact and robust would be a very important scientific tool for researchers working in the mid-infrared (mid-IR).

Applications such as differential absorption LIDAR and coherent optical communications require both narrow linewidths and high average power in the mid-IR. The most effective way to meet both of these requirements is to injection-seed a high-power pulsed OPO. A highly monochromatic tunable diode-pumped OPO is the most cost effective tool for this application.

2 INTRODUCTION

The parametric oscillator is an efficient and potentially compact device for generating mid-infrared wavelengths. The most common pump lasers for OPO's are Nd:YAG and Ti:Sapphire lasers. The narrow linewidth and highly stable output make them exceptionally good pump sources. However, they are also very large and inefficient. For a compact system, the diode laser is a very good candidate if it can be fabricated to meet the requirements of narrow linewidth, single mode operation with an adequate output power for the application. In our Phase I effort, we identified the monolithic master oscillator power amplifier (MOPA) diode laser made by Spectra Diode Laboratories, Inc. (SDL) as the pump source for a continuous wave diode-pumped OPO. The SDL product literature listed specifications for the MOPA that fit within our requirements for a diode laser source. We proceeded with a Phase II effort to build and deliver a diode-pumped OPO (DPOPO) to Phillips Laboratory. During the course of the contract we acheived the first reported operation of a CW DPOPO, using a periodically poled lithium niobate crystal (PPLN). The technical results of this work are significant, however a stable device could not be delivered to the government due to uncontrollable instabilities in the SDL MOPA. A full characterization of the MOPA operation is contained in this report.

The technical issues that needed to be addressed under this contract were to develop multi-chroic coatings for the optics in the OPO cavity, develop and refine the electric field repoling of LiNbO$_3$, and to develop a rigorous theoretical model for tightly focused Gaussian beams in OPO cavities. All of these issues progressed well enabling Cygnus Laser to design and build a prototype that will operate succussfully when a new diode laser source is identified.

3 DROPO MODELING RESULTS

We have developed a straightforward but descriptive analytic model of a low-power continuous-wave diode-pumped (CWDP) doubly-resonant optical parametric oscillator (DROPO). We have found (by comparison with selective numerical tests) that for a low-loss, low-gain system, the backconversion effects which result from imperfect phase-matching (which arises naturally in systems of interacting nonuniform fields[1, 2]) do not play a significant role in the determination of the operating characteristics of the CWDP-DROPO. Instead, the primary effect of pump, signal, and idler beam nonuniformity is the well-known reduction of the threshold pump power—and the corresponding increase in the conversion efficiency—provided by an optimally focused pump field.[3] We have found that even under optimal conditions these effects are mitigated considerably if the pump field is not Gaussian (such as the pump beam provided by the diode laser in this experiment).

Consider, then, a system of three interacting electromagnetic fields with wavelengths satisfying both the inequality $\lambda_1 \geq \lambda_2 \geq \lambda_3$ (allowing the identifications $1 \equiv$ idler, $2 \equiv$ signal, and $3 \equiv$ pump), and the equality $1/\lambda_3 = 1/\lambda_1 + 1/\lambda_2$. Writing out each wave equation in turn, we have a set of first-order coupled ordinary (i.e., time-independent) nonlinear differential equations that describe the evolution of each frequency component in space as it propagates

through the nonlinear optical medium:

$$\frac{d}{dz}E_1(z) + \frac{\alpha_1}{2}E_1(z) = i\frac{\omega_1}{n_1 c}d_{\textit{eff}}E_2^*(z)E_3(z)e^{i\Delta kz}, \tag{3.1a}$$

$$\frac{d}{dz}E_2(z) + \frac{\alpha_2}{2}E_2(z) = i\frac{\omega_2}{n_2 c}d_{\textit{eff}}E_1^*(z)E_3(z)e^{i\Delta kz}, \text{ and} \tag{3.1b}$$

$$\frac{d}{dz}E_3(z) + \frac{\alpha_3}{2}E_3(z) = i\frac{\omega_3}{n_3 c}d_{\textit{eff}}E_1(z)E_2(z)e^{-i\Delta kz}, \tag{3.1c}$$

where ω_m, n_m, and α_m are the angular frequency, refractive index, and linear background absorption coefficient, respectively, of field m, and

$$\Delta k \equiv k_3 - k_1 - k_2 = \frac{\omega_3}{c} - \frac{\omega_1}{c} - \frac{\omega_2}{c} = \frac{2\pi n_3}{\lambda_3} - \frac{2\pi n_1}{\lambda_1} - \frac{2\pi n_2}{\lambda_2}. \tag{3.2}$$

Next, we cast the wave equations (3.1a)–(3.1c) into a simpler form [4]. First, we define the normalized amplitudes of the three interacting fields as

$$A_1(z) \equiv \sqrt{\frac{1}{2}n_1\epsilon_0 c}\,E_1(z), \tag{3.3a}$$

$$A_2(z) \equiv \sqrt{\frac{1}{2}n_2\epsilon_0 c}\,E_2(z), \text{ and} \tag{3.3b}$$

$$A_3(z) \equiv -i\sqrt{\frac{1}{2}n_3\epsilon_0 c}\,E_3(z). \tag{3.3c}$$

Note that the intensity of field m is now given by $I_m(z) = |A_m(z)|^2$. Since $\omega_m \equiv 2\pi c/\lambda_m$, if we assume that the bulk loss of the nonlinear optical crystal is small compared to the applied multichroic antireflection coatings, we can write the differential wave equations (3.1a)–(3.1c) as

$$\frac{d}{dz}A_1(z) = -CA_2^*(z)\,A_3(z)\,e^{i\Delta kz}, \tag{3.4a}$$

$$\frac{d}{dz}A_2(z) = -\Lambda CA_1^*(z)\,A_3(z)\,e^{i\Delta kz}, \text{ and} \tag{3.4b}$$

$$\frac{d}{dz}A_3(z) = (1+\Lambda)CA_1(z)\,A_2(z)\,e^{-i\Delta kz}, \tag{3.4c}$$

where

$$\Delta k \equiv k_3 - k_1 - k_2, \tag{3.5}$$

$$\Lambda \equiv \lambda_1/\lambda_2, \text{ and} \tag{3.6}$$

$$C \equiv \sqrt{\frac{8\pi^2}{\epsilon_0 c}}\,\frac{d_{\textit{eff}}}{\lambda_1\sqrt{n_1 n_2 n_3}}. \tag{3.7}$$

The effort needed to solve (3.4a)–(3.4c) depends on the boundary conditions chosen. In general, solutions in the case of critical phase-matching (i.e., $\Delta k \neq 0$) are difficult to obtain

4

analytically. However, we are specifically interested in devices with high output powers in the 3–5 μm wavelength range. Therefore, we assume that the reflectivity of the output coupler is nearly 1 at the signal wavelength, or $T_2 \ll 1$, and we neglect the variation of the signal field A_2 over the length of the nonlinear optical crystal. This reduction in the number of free fields allows us to find a tentative solution for a single pass of the pump and idler fields through the optical parametric amplifier:

$$A_1(z) = \left[A_1(0) \left(\cos \gamma z - i \frac{\Delta k}{2\gamma} \sin \gamma z \right) - A_3(0) \frac{C A_2^*}{\gamma} \sin \gamma z \right] e^{i\Delta kz/2}, \text{ and} \qquad (3.8a)$$

$$A_3(z) = \left[A_3(0) \left(\cos \gamma z + i \frac{\Delta k}{2\gamma} \sin \gamma z \right) + A_1(0) \frac{(1+\Lambda)C A_2}{\gamma} \sin \gamma z \right] e^{-i\Delta kz/2}, \qquad (3.8b)$$

where

$$\gamma^2 \equiv (1+\Lambda)C^2 I_2 + \left(\frac{\Delta k}{2} \right)^2, \qquad (3.9)$$

and $I_2 \equiv |A_2|^2$.

In the case of single-pass pumping, we apply the Maxwell boundary conditions to the idler field, requiring that $A_1(L_c)r_1 \exp(i\phi_1) = A_1(0)$, where $\exp(i\phi_1)$ is the additional phase accumulated by the idler carrier wave as it propagates around the resonator. If we first solve (3.8a) for $A_1(0)$ using this boundary condition, substitute the result and (3.8b) into (3.4b), and then apply the boundary condition $A_2(L_c)r_2 \exp(i\phi_2) = A_2(0)$, where L_c is the crystal length and r_2 is the electric field reflection coefficient for λ_2, we obtain

$$\frac{2}{\Lambda C^2 L_c^2 I_p} \left[\frac{\exp(i\phi_2)}{r_2} - 1 \right] = \frac{1}{\zeta} \left[1 - (1-\delta^2)\sin^2(\zeta)|Q|^2 \right] \left\{ \zeta \text{sinc}^2(\zeta) + i\delta \left[1 - \text{sinc}(2\zeta) \right] \right\}$$
$$+ 2Q^* \text{sinc}^2(\zeta)[\cos(\zeta) + i\delta \sin(\zeta)]$$
$$- (Q - Q^*)\text{sinc}(\zeta)[1 - \text{sinc}(2\zeta)](1 - \delta^2)$$

$$(3.10)$$

where $\zeta \equiv \gamma L_c$, $\delta \equiv \Delta k\, L_c/2\zeta$, I_p is the pump intensity and

$$Q \equiv \frac{r_1 \exp[i(\Delta k\, L_c/2 - \phi_1)]}{1 - r_1 \exp[i(\Delta k\, L_c/2 - \phi_1)][\cos(\zeta) - i\delta \sin(\zeta)]} \qquad (3.11)$$

We have studied (3.10) numerically, and we have found the surprising result that the effects of a net nonzero wavevector mismatch arising from the use of nonuniform beams can be neglected in carefully aligned devices where both the reflection losses and the parametric gain are small. We therefore consider the optimum case where the resonator length has been tuned to the coincident resonance of both the signal and the idler (i.e., $\exp(i\phi_1) = \exp(i\phi_2) = 1$), and the wavevector mismatch Δk has been reduced to zero. By simplifying (3.10), we then obtain the simple transcendental equation

$$\frac{P_3}{P_{th}} = \frac{2}{(1+r_1)r_2} \left[\frac{1 - r_1 \cos(\zeta)}{(1-r_1)\text{sinc}(\zeta)} \right]^2, \qquad (3.12)$$

5

where now $\zeta \equiv [2(1 + \Lambda)C^2 L_c^2 P_2 / \pi w_2^2 T_2]^{1/2}$, P_2 is the signal output power, w_2 is the signal beam waist radius, and T_2 is the signal output power transmission coefficient.

The threshold power P_{th} can be found by equating the single-pass parametric gain to the round-trip amplitude loss; we obtain

$$P_{th} \approx N_p^2 \frac{\pi w_3^2}{2} \frac{(1 - r_1)(1 - r_2)}{\Lambda C^2 L_c^2}, \qquad (3.13)$$

where w_3 is the pump beam waist radius and N_p is the pump beam quality factor (expressed as the "number of times the diffraction limit"). We have added the phenomenological factor N_p^2 based on numerical studies of (3.10) with non-Gaussian fields. Note that we have *not* included a similar factor in ζ, because the resonator length which enhances the lowest-order Gaussian signal mode is not the same as the lengths which support the higher-order modes, due to differences in the Guoy phases of each mode.

Equation (3.12) allows a straightforward computation of the signal output power as a function of the pump power incident on the PPLN. We simply compute the pump power required to achieve a given signal output power for a range of output powers of interest, and then transpose the result. Applying this method to the parameters listed in Table 1 for the degenerate DROPO results in the curve shown in Figure 3.1, which is in reasonable agreement with experimental results. There is a factor of two discrepancy between the output power predicted by the model and the experimental data, however this is a result of degenerate operation in which the signal and idler wavelengths are nearly identical, doubling the expected output power of the OPO.

4 EXPERIMENTAL RESULTS

4.1 KTA OPO Experiment

The KTA OPO work was discontinued under this contract. Several attempts were made to obtain parametric oscillation with the original crystal from Phase I, however no output was observed. A Ti:Sapphire operating at 960 nm with 315 mW of output power was tried without success. A second attempt with an SDL MOPA operating at 960 nm with an output power of 470 mW and single mode operation also failed to produce a detectable output from the crystal. No further attempts were made with KTA and this work was halted with permission from Phillips Laboratory.

4.2 PPLN Crystal Development

4.2.1 Stanford Subcontract

The development of electric field repoling of lithium niobate (PPLN) performed at Ginzton Laboratory was very successful. Several samples of PPLN were produced which exhibited a high degree of uniformity of domain inversion over an interaction length of up to 15 mm. Three samples were prepared for Cygnus Laser to use in OPO experiments. The PPLN was fabricated with a 28.5 μm period suitable for 1.96 μm generation when pumped with a 980 nm

Table 1: Computed Model Input Parameters

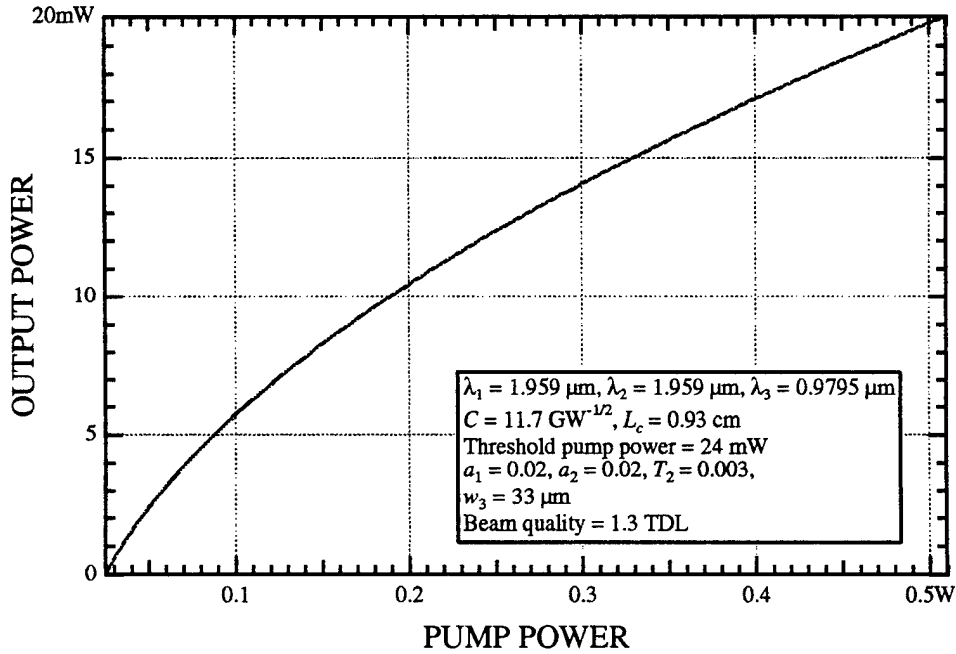| Description	Symbol	Value	Units
PPLN crystal length	L_c	0.93	cm
Round-trip idler power loss $(1 - r_1)$	a_1	0.02	
Round-trip signal power loss $(1 - r_2)$	a_2	0.02	
Signal output power coupling	T_2	0.003	
Pump waist radius	w_3	33	μm
Beam quality	N_p	1.3	
Effective nonlinear optical constant	C	11.7	GW$^{-1/2}$

Figure 3.1: Output power curve computed by solving and transposing (3.12) using the parameters listed in Table 1.
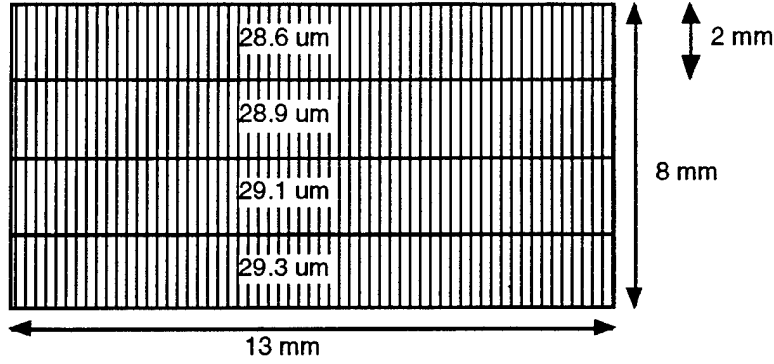
Figure 4.1: Multi-period PPLN fabricated by Crystal Technology.

MOPA laser diode. Of these three crystals, only one remains usable and has demonstrated OPO activity. One was optically damaged at Ginzton Laboratory and the third developed a crack perpendicular to the beam path and cannot be used. The PPLN fabrication at Ginzton Laboratory is detailed in a Final Technical Report attached as Appendix A.

4.2.2 Crystal Technology PPLN Fabrication

A license for the PPLN fabrication technology was granted to Crystal Technology in California. Cygnus Laser purchased three PPLN samples from Crystal Technology for both degenerate and nondegenerate operation with a 980 nm and 1.064 μm pump laser. Three pieces were purchased and delivered from their first stock runs. Two pieces contain four regions, each with a different periodicity, while the third has a periodicity of 30 μm. The domain pattern for the multi-period samples is shown in Figure 4.1. The periods for the multi-period pieces—28.6 μm, 28.9 μm, 29.1 μm and 29.3 μm—were chosen by Crystal Technology to phase match a Nd:YAG pump at 1.064 μm. Only the 28.6 μm period is short enough to reach the 3-5 μm wavelength region when used with the 979 μm MOPA pump source. Cygnus Laser ordered the PPLN from stock runs as test samples to examine the uniformity of poling from Crystal Technology's fabrication process. We found the pieces to be acceptable, however they did not exhibit the same degree of uniformity seen in the PPLN fabricated by Larry Myers. There is more variation in the duty factor (thickness of the domains), and many of the domain walls zigzag by as much as one half the domain thickness. These effects are more pronounced in the multi-period pieces than in the 30 μm piece. It should be noted that these are first run samples and Crystal Technology is actively refining their repoling process to ensure uniform pieces on a commercial production scale.

The two multi-period pieces were coated for nondegenerate operation by Lightning Optical and are ready for testing. However, due to the instabilities encountered with the SDL MOPA, further experimentation cannot be performed at this time. Cygnus Laser will not actively develop more PPLN with Crystal Technology until a suitable pump source has been identified, since the periodicity of the PPLN is designed to phase match to a specific pump wavelength.

8

4.3 Trichroic Coating Development

4.3.1 Overview

Lightning Optical Corporation was contracted to design and fabricate a triple Anti-Reflection (AR) coating on $LiNbO_3$ for the wavelengths of 3.39 μm, 1.39 μm and 0.980 μm. The widely spaced spectral lines over which the coating is required to work and the high damage threshold that is required limited the materials available for fabrication of the AR coating. After initial literature searches and testing, a six layer five-material design was selected that attained or exceeded all performance criteria. The modeled performance of the designed coating is shown in Figure 4.2. This meets the criteria of reflectance less than 0.5% at 3.39 μm and 1.39μm and less than 2% reflectance at 0.98 μm. The broad low reflectance region of the coating at 3.39 μm is highly tolerant of dispersion in the coating materials allowing the coating performance to be tuned to the 1.39 μm and 0.98 μm lines without sacrificing performance at 3.39 μm. The coating is designed to have maximum tolerance of deposition errors thereby increasing yield expectations of production fabrication. Based on $\pm$3% layer thickness accuracy the expected maximum reflection at 1.39 μm due to coating fabrication error is 0.75% and 4% at 0.98 μm. The broad response of the coating at 3.39 μm means a better tolerance of coating errors than at the shorter wavelengths with the maximum reflection rising to approximately 0.35% for the maximum production error.

4.3.2 Coating Production

The previously designed coating was deposited on $LiNbO_3$ samples in January 1995 and sent to Cygnus Laser for evaluation. At the time of the deposition Lightning Optical Corporation did not have the capability to measure reflectance beyond 3.2 μm but extrapolated that the reflectance was low based on the slope from 2.8 μm to 3.2 μm and the position of the near IR peaks. Measurements made for Cygnus Laser indicated that the reflectance at 3.39 μm was very high, approximately 10%. The parts were sent back to Lightning Optical Corporation where they were measured in reflection from 2 μm to 5 μm by another vendor with reflectance measurement capabilities. The measurement showed the reflectance to be less than 0.25% and centered at 3.39 μm. The reflectance of the coated $LiNbO_3$ sample from 0.9 μm to 1.6 μm is shown in Figure 4.3 and the reflectance of the sample from 2 μm to 5 μm is shown in Fig. 4.4. All measurements showed the coatings to meet the low reflectance requirements.

4.3.3 Laser Damage and Lifetime

Formal laser damage testing was not performed on the $LiNbO_3$ samples coated by Lightning Optical Corporation. The coatings have been in use at Cygnus Laser. Under repeated use the coated samples have performed well. There is evidence of damage to the surface of the optic but the cause is likely to be contamination of the surface which subsequently burned causing the damage to the optic and is not due to coating failure. Continued use of the optics supports this conclusion. Additionally, the continued use of the coated optic for a period approaching one year indicates that the coating has no aging degradation. All indications are that the coating performs to specifications and is not subject to laser induced damage in the
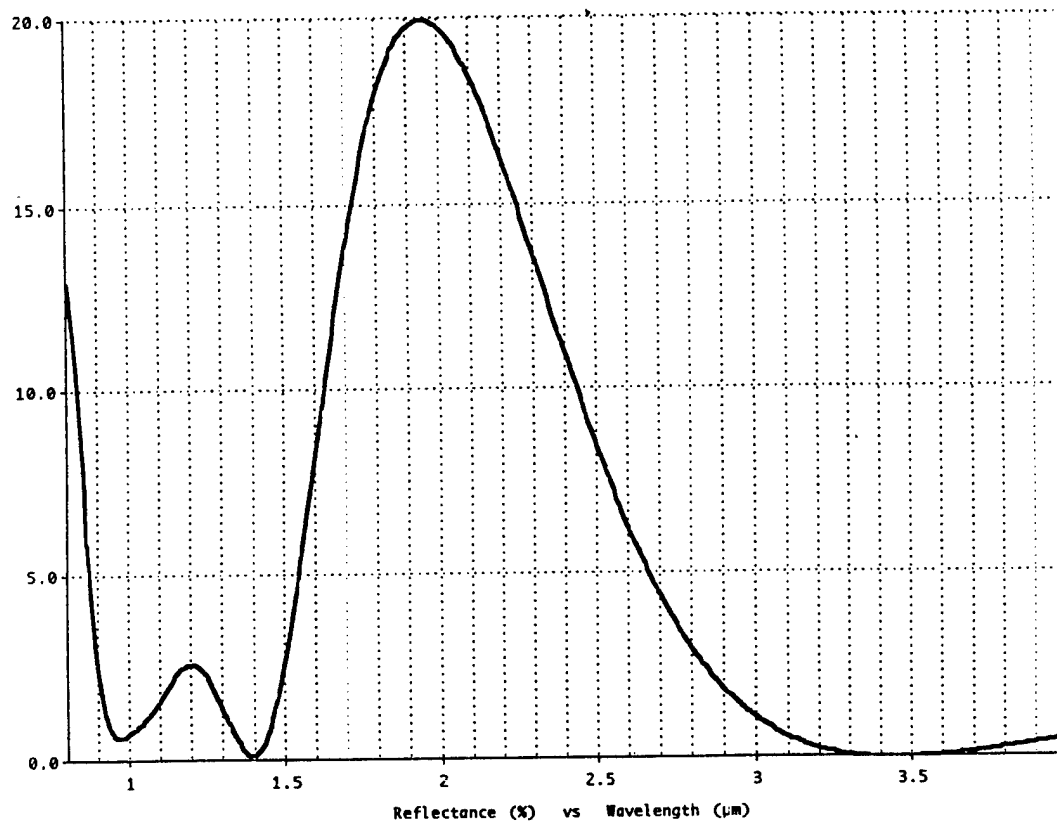
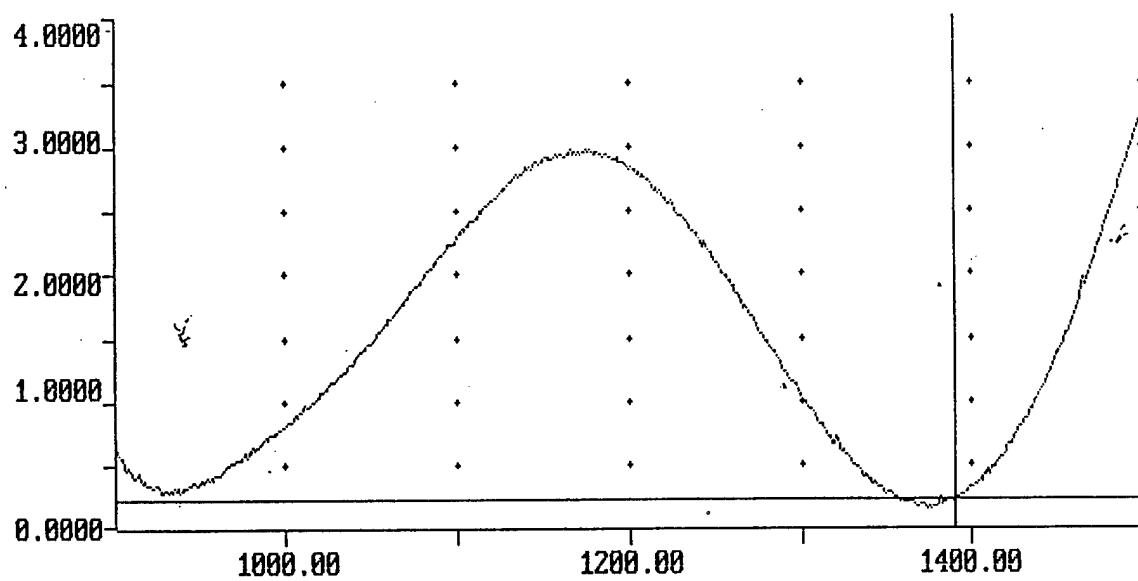Figure 4.2: Modeled performance of the triple AR coating.

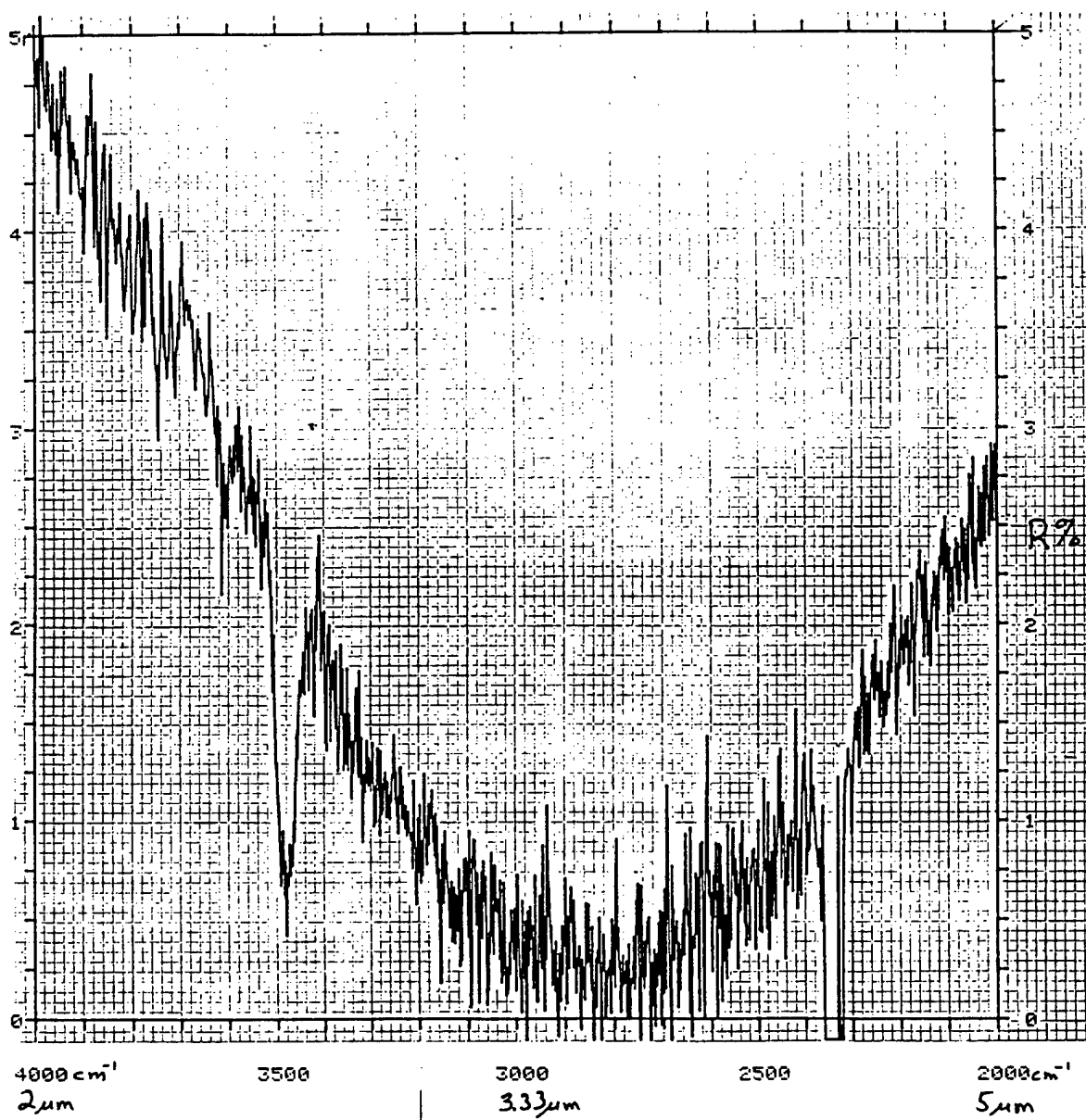Figure 4.3: Near IR reflectance of the triple AR coating deposited on LiNbO$_3$.

Figure 4.4: Mid-IR reflectance of the triple AR coating deposited on LiNbO$_3$.

operating environment and appears to have no lifetime degradation. Proof of reproducibility and production yield has not been established.

4.4 Diode-Pumped OPO Experiment

4.4.1 Doubly Resonant Degenerate OPO Results

We obtained a possibly significant result with the diode-pumped CW OPO under this Phase II contract—spectrally stable output from the OPO that showed no cluster effect. A laser with a narrow linewidth is critical for CW OPO operation for a very important reason—minor spectral fluctuations in the pump laser will cause the OPO to hop between different signal-idler clusters that satisfy the conservation of energy. This effect was clearly seen in the work performed at Stanford using MOPA-1. Figure 4.5 shows the output from the CW DROPO running in a degenerate mode. Note the several peaks that appear as the piezo stage was translated through a range of 70 nm. The cluster effect occurs when the pump laser linewidth is broad enough to allow several different signal-idler pairs to resonate as the cavity is translated. This means that as the cavity length changes, the wavelength of the signal and idler change. This change in wavelength was observed in the output shown in Figure 4.5. If a stable CW OPO device is to be used for applications where a specific wavelength is needed, the cluster effect will interfere with the collection of data. However, in our experiments at Cygnus Laser using MOPA-2, this cluster effect was not observed at all. An oscilliscope trace of the degenerate operation of the OPO is shown in Figure 4.6. The piezo stage was scanning over a 10 μm distance and peaks were seen as the stage moved into resonance approximately every 1.95 μm. The important thing to note here is that the wavelength of the signal and idler did not change as the cavity mirror was translated. In this case, a spectrally stable output was achieved. This is a very significant result. It verifies the benefit of a narrow linewidth source and shows that a CW OPO can be made without the negative effects of signal-idler clusters. To our knowledge, this is the first time this effect has been demonstrated with a CW diode-pumped OPO. A drawing of the layout of the OPO experimental setup is shown in Figure 4.7.

Additional data to corroborate this phenomenon would be beneficial. Spectral analysis to confirm this effect was not done because the MOPA was no longer operational at the time the effect was analyzed.

The diode pumped OPO experiment did not progress at the rapid pace that we anticipated due to instabilities in the SDL laser diode MOPA's. A diode pumped OPO requires a laser source that has several key features: single longitudinal mode operation, narrow spectral linewidth (<25 MHz), and a highly coherent wavefront, all with long term stability. Cygnus Laser had three SDL MOPA's (identified as MOPA-1, MOPA-2 and MOPA-3) for use in this Phase II effort and all have serious problems that prohibited further development of the CW diode-pumped OPO.

The first laser delivered, MOPA-1, operated on a single longitudinal mode for short periods of time and occassionally became unstable, operating in a broadband mode. The tendency to run on several modes necessitated a technician to constantly monitor the output of a scanning fabry perot interferometer placed in the beam path, adjusting the oscillator or amplifier current as necessary. Parametric oscillation was achieved with this laser over very
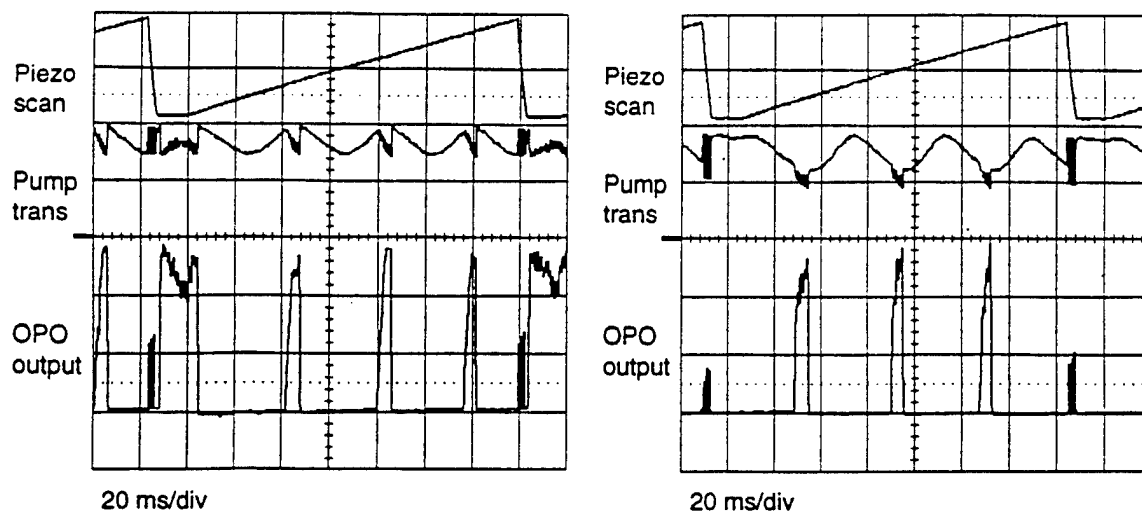
Figure 4.5: OPO output showing the cluster effect when pumped with the broader linewidth MOPA. Trace 1 is the piezo ramp and trace 2 is the OPO output.
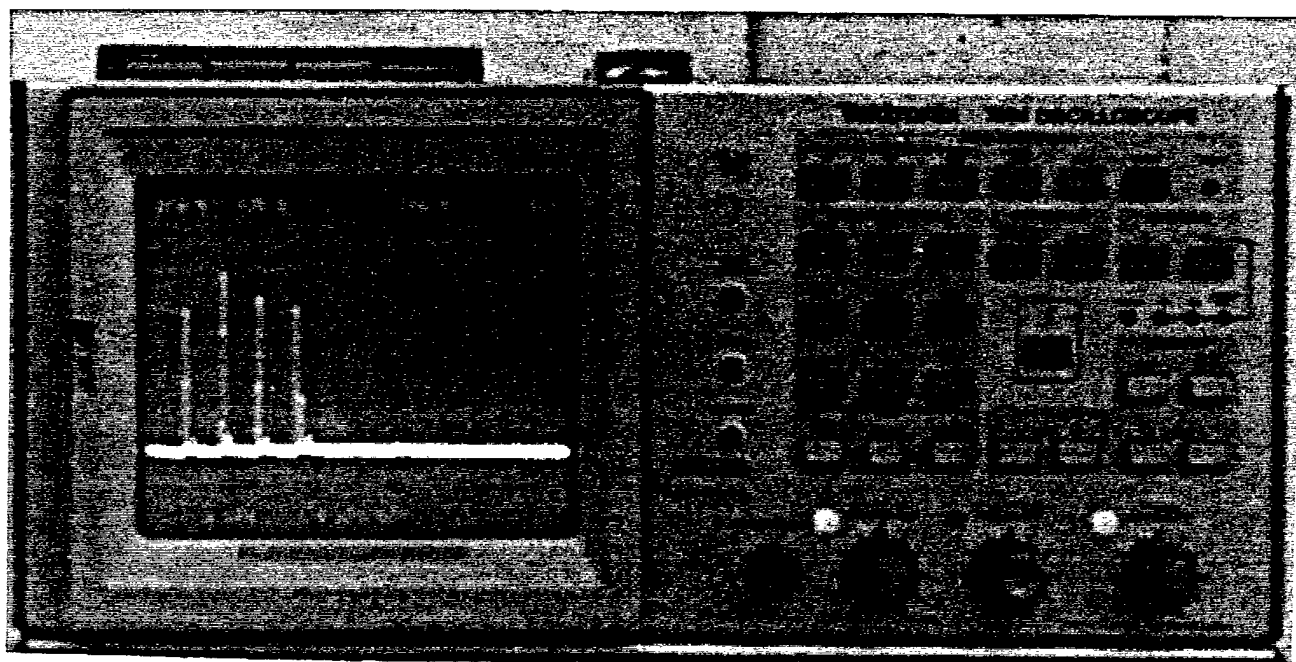

Figure 4.6: OPO output showing absence of the cluster effect when pumped with the narrower linewidth MOPA.
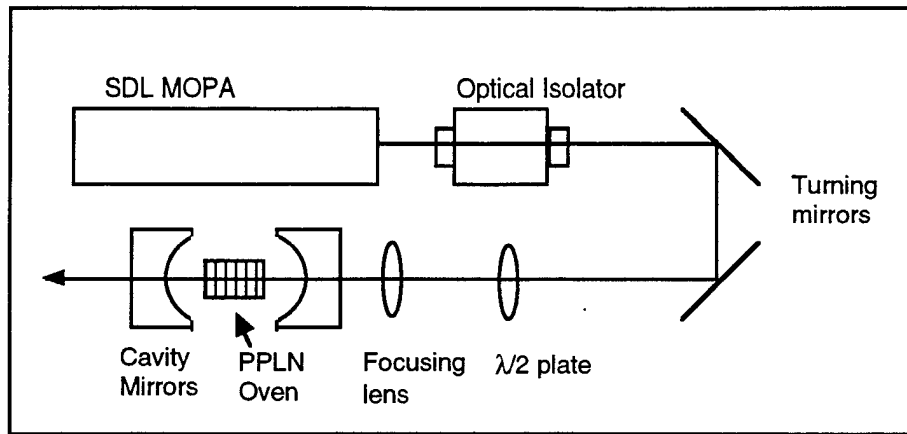
Figure 4.7: Experimental setup of the diode-pumped doubly resonant OPO.

short periods, however it was impractical for use in the laboratory and could never be part of a delivered unit. The behavior of this laser was characterized in the first two quarterly reports.

We took delivery of MOPA-2 from SDL in April of 1995. This MOPA was used for PPLN experiments at Stanford, although they were not able to achieve oscillation. We believe it was a matter of misalignment of the cavity optics rather than a fault with the MOPA at that time. The joint experimentation with Stanford ended in June of 1995 and all the optical equipment was taken to Cygnus Laser for further development. In December of 1995, a degradation of optical output power occurred in MOPA-2 during normal operation. The unit was sent to SDL for diagnosis and it was found that an optical element had shifted. SDL mounted the optics in the first MOPA's with an epoxy that was not appropriate for mounting position sensitive elements requiring long term stability. They experienced problems with many of the first units and later corrected the problem by using a different epoxy. SDL realigned the shifted element and returned MOPA-2 to us on the 27th of December. We characterized the new beam profile and adjusted the OPO setup to mode match this beam. On January 30, 1996 we achieved oscillation with the OPO operating in a degenerate mode. The OPO had a threshold of 105 mW with an output power greater than 11 mW—the saturation level of the InAs detector. The OPO operated over the course of a week with an unstable output. Air currents, temperature gradients and light pressure on the optical table all strongly affected the phase matching conditions inside the PPLN, causing erratic output. We reasassembled the cavity, replacing the critical component mounts with a more thermally and vibrationally stable configuration. During the two week down time of the OPO while parts were being machined, the optics in MOPA-2 shifted once more, degrading the output of the laser to a point at which no OPO activity could be generated. As of the writing of this final technical report, we still do not have a stable MOPA laser for CW diode-pumping of an OPO.

4.4.2 Defective Operation of the MOPA

The concept of a stable CW diode-pumped OPO was based on the assumption that the most critical aspects of frequency stabilization and linewidth narrowing were successfully

addressed by SDL in their monolithic master oscillator power amplifier. The monolithic distributed feedback oscillator and tapered amplifier architecture was the most stable commercial solution to the very difficult task of setting up a feedback mechanism for single frequency operation of a high powered diode laser. The research team at SDL was able to engineer a MOPA that operated on a single longitudinal mode, with a linewidth less than 25 MHz. However, we have learned that these characteristics were not obtainable on a commercial production scale.

A very specific set of circumstances must be met in order for a MOPA to run single frequency. The physical parameters that govern this set of specifications cannot vary with environmental fluctuations or operating conditions. It is apparent that the MOPA specifications outlined in the SDL catalog for model number SDL-5762-A6 were characteristic of a small percentage of units sold by SDL. The product literature published by SDL states that the MOPA is a single longitudinal mode, TEM_{00}, 750 mWatt diode laser with a linewidth <25 MHz. Cygnus Laser and Phillips Laboratory contracted with SDL to deliver two MOPA's that were best of lot over a six month period (Phillips Laboratory purchase order number F29650-94-ML600). SDL would characterize the MOPA's as they came out of production and place the two best units on a shelf. If a superior unit was manufactured, it would then replace one of the held units, and the process would continue with a final delivery of the two best units of the six month period to Cygnus Laser. We were asking for two simple things from SDL—a product that met *their specifications*, and was a best effort specimen from a standard production run.

The first unit delivered under the purchase order (MOPA-2) was characterized by SDL to have a linewidth less than 1 MHz when the oscillator current was set to 170 mAmps and the amplifier current was varied from 1.7 Amps to 2.2 Amps, and from 2.4 Amps to 2.6 Amps. Single longitudinal mode operation was verified at Cygnus Laser with a simple etalon. The MOPA operated on a single longitudinal mode over the entire amplifier current range above lasing threshold. The interferogram remained sharp as the amplifier current and temperature were modulated, indicating that it maintained a narrow linewidth. We operated this MOPA without incident for a period of five months.

During its sixth month of use, the MOPA triggered a safety shutdown while operating under normal conditions. The power supply that drives the MOPA is an ILX unit specifically designed for use with the SDL MOPA's. A power limit safety feature was set on the driver that automatically shuts off the current to the amplifier when it detects an output power above a specified level. We restarted the MOPA after the unexplained shutdown, and measured a decreased output power of approximately 25%. We shipped the unit to SDL for diagnosis and found that an element in the beam conditioning optics inside the MOPA had shifted. This caused a disproportionate amount of light to fall on the monitor photodiode (MPD) at the exit port of the housing, thus degrading the output and changing the calibration of the MPD. The first MOPA's from the production line suffered from similar problems due to a poor choice of epoxy for cementing the optics. SDL recemented the optic with a new epoxy and shipped the unit back. We tested the reconditioned MOPA-2, found it to meet our requirements and reassembled the OPO cavity based on the new beam radius.

After several weeks of unsuccessful attempts to acheive parametric oscillation, we noticed an aberration in the beam. We removed all elements in the pump beam path and examined the beam with a diverging lens. A diffraction pattern was strongly evident across the hori-
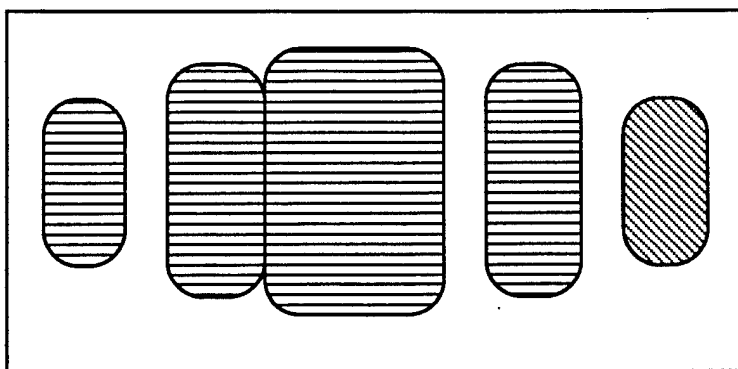
Figure 4.8: The near field pattern of the aberrated MOPA beam.

zontal plane of the MOPA indicating that the beam inside the MOPA housing was no longer focussed on the internal 60 μm slit in the center of the housing. We expanded the beam to approximately 15 cm and detected another anomaly. A very fine interference pattern could be seen across the vertical plane similar to Figure 4.8. These factors disrupted the coherency of the wavefront and prevented further parametric oscillation. We sent MOPA-2 back to SDL on March 1, 1996 for further analysis.

The MOPA is fabricated as a permanent unit and is not easily repaired. The removal of an optic inside the housing can disrupt the feedback to the diode laser and render it unusable. For these reasons, SDL preferred to fabricate a new MOPA for Cygnus Laser rather than attempting to repair MOPA-2. Randy Klein, the contact for Cygnus Laser at SDL, agreed to manufacture a new MOPA that met the same specifications outlined in the original purchase order. Cygnus Laser received the replacement MOPA (MOPA-3) on May 3, 1996. Test data on the specifications of MOPA-3 were not included with shipment of the laser. We tested the laser for single mode operation with a simple etalon and found that it operated on multiple longitudinal modes over all current ranges. It had a highly unstable bandwidth, changing from narrow to broadband with every 0.01°C. We phoned SDL and spoke with Dave Evans, Vice President of production and Randy Klein's superior. He stated that SDL could not meet the specifications in the purchase order for another unit, indicating that it was not feasible to test production units for operation within the specifications outlined in their catalog. We were also informed by SDL that the second unit ordered by Phillips Laboratory on Customer Order No. F29650-94-ML600 had been canceled by Phillips Laboratory. We were not made aware of this by our contract monitor. Our solution to the situation was to have MOPA-2 repaired by SDL on a best effort basis, realizing that it may not retain its narrow linewidth and single mode operation. We received the reconditioned MOPA-2 on May 14, 1996. Its linewidth is stable, however it is now a multiple longitudinal mode laser over all current settings. Without a suitable laser diode source, we could not proceed with design of a nondegenerate OPO, and we are not able to test the stability of the isolation system we designed for long term operation of a CW diode-pumped OPO.

17

4.5 OPO Alignment Procedure

The alignment procedure for a doubly resonant OPO is detailed in common sources explaining OPO theory. We spent considerable effort designing an alignment procedure that was efficient and accurate. This section is included as a tutorial for determining the correct placement of OPO cavity optics.

4.5.1 MOPA Characterization

The SDL MOPA is a new laser that has not yet enjoyed thorough field testing and burn-in prior to its emergence in the commercial market. We have characterized a handful of MOPA's and found them all to have certain aberrant behavior under normal operating conditions. It is imperative that any MOPA used in a phase or intensity sensitive design be carefully and thoroughly analyzed and continually monitored to ensure that the beam is uniform with time.

The CW doubly resonant OPO is extremely sensitive to wavelength and to wavefront coherence. There are several methods of determining the stability of a laser source. First, one must check for single frequency operation by setting up an etalon and viewing the ring pattern. To do this, pick off a portion of the pump beam with a quartz window, expand the beam with a diverging lens and place a fabry-perot etalon near the lens. Turn the MOPA on to half power and rotate the etalon until a uniform ring pattern appears on the viewing screen. Vary the current slowly from minimum to maximum operating limits. The ring spacing will vary slowly with current, however no more than one mode should operate at one time. If a point is reached where instability is noted, the oscillator current can be changed by several milli-amperes to see if the mode pattern will stabilize. The linewidth of the MOPA should also be characterized. For the DROPO the linewidth must less than 25 MHz. If the MOPA is unstable or does meet the linewidth requirement, it will not be an appropriate source for stable parametric continuous wave oscillation and another source should be found.

4.5.2 Mode-Matching Calculations

If the MOPA does meet specification, the isolators and turning mirrors can be put in the setup in their respective places consistent with the dimensions and spacing of the final product. Because the MOPA is not perfectly collimated, it is critical that the OPO layout resemble the final product and that the optical elements are not grossly repositioned after beam measurements are made. We found that different isolators will change the diameter of the beam, thus reinforcing the point that assumptions based on perfectly collimated beams do not necessarily apply to real beams.

After the isolator and turning mirrors have been inserted and aligned, view the beam with an IR camera to make sure that it is centered on each element and that no structure has been introduced into the beam from clipping or misalignment. The Isowave isolator typically has a 0.6 dB loss and the aluminum mirrors have a 0.2 dB loss each. Measure the power loss after each element and adjust positions accordingly without disturbing the beam profile.

Next, measure the beam diameter to determine the proper positions of the lenses for mode matching to the cavity. The curvature of the wavefront must be matched to the curvature of

the cavity mirror through the confocal parameter. This is accomplished by focusing the pump beam with a plano-convex lens and placing the cavity mirror at a specified distance from the focal point where the curvature of the lens and the beam are nearly identical. The first step in calculating the mirror positions is to measure the beam diameter where the focusing lens will be inserted. In our experiments we mounted a razor blade on a 3-axis translation stage from Newport equipped with sub-micron resolution differential micrometers. Other methods in which sub-micron resolution can be achieved will work as well. Measure the beam in **both** the horizontal and vertical planes.

The power of the focusing lens can be approximated using standard ray tracing theory. The optimum pump, signal and idler wave radii are determined by balancing the minimization of oscillation threshold with the need to stay below the optical damage threshold of the PPLN crystal. These parameters are given in the OPO modeling section of this report. The cavity mirrors for the OPO being developed under this contract have a radius of curvature of 1 cm and the MOPA beam radius is approximately 1.5 mm. Based on these parameters the focal length of the lens should be ≤ 50 mm.

Insert the $\lambda/2$ waveplate, the polarizing cube and the 50.2 mm plano-convex (PCX) lens (or focusing lens) into the beam path. Attach the razor blade to the translation stage for vertical scanning. Place the translation stage after the PCX lens and scan across the beam, taking measurements at the $1/e^2$ points of maximum power (14% and 86%). Take measurements approximately every 5-10 mm beginning with the razor blade next to the PCX lens through twice the focal length of the lens. Since the beam is tightly focused at the focal point, the razor blade edge will cause diffraction, making the near field data inaccurate. However, it is still useful for determining the focal point for each direction. The far-field measurements are the most important because the razor blade will not noticeably spread the beam. Repeat this procedure in the horizontal direction. Be aware that the vertical and horizontal components of the beam may focus at different points in space—neither of which will be at the focal point of the lens in the product literature.

The equation for a Gaussian beam radius is

$$w(z) = w_0 \sqrt{1 + \frac{\lambda(z - z_0)^2}{\pi w_0^2}} \tag{4.1}$$

where w_0 is the beam waist radius at the focal point z_0, z is the distance from the focal point and λ is the pump wavelength. Plot the beam data and find the actual waist of the beam with a curve fit function (a sample curve fitting program for Mathcad is included in Appendix B). Plot both the data and the curve predicted by Eq.(4.1) on the same graph. If the two curves are shifted, adjust the focal point in Eq.(4.1) until a good overlap is achieved and use this value as the actual focal point of the lens. If the horizontal and vertical waists differ by more than 2 microns, a radial waist must be approximated and used for the mode matching calculations. The equation for the radial waist is

$$w_r = \sqrt{\frac{1}{2}(w_h^2 + w_v^2)} \tag{4.2}$$

where $w_{h,v}$ are the horizontal and vertical waist radii, respectively, and the focal point for w_r is midway between that of the two waists. It is not unusual for the calculated waist to be

19

as much as 2-3 times larger than the scanned waist measurement, due to diffraction induced losses at the focal point.

The next step is to find the width and position of the OPO cavity for which the pump beam and cavity mode will match. We will use ray tracing theory for this calculation. The expression for $q(z)$, the complex beam parameter for a Gaussian beam is

$$\frac{1}{q(z)} = \frac{1}{R(z)} - j\frac{\lambda}{\pi w^2(z)} \tag{4.3}$$

where

$$R(z) = z\left[1 + \left(\frac{\pi n w_0^2}{\lambda z}\right)^2\right]. \tag{4.4}$$

The complex beam parameter for a beam that has been optically transformed is given by

$$q_2(z) = \frac{Aq(z) + B}{Cq(z) + D} \tag{4.5}$$

where A, B, C and D are the matrix elements of the transforming system. For the OPO, we will let $q(z)$ represent the beam at the focal point of the 50 mm focusing lens. At this point, the radius of curvature of the wavefront, $R(z)$, is equal to infinity. This reduces Eq.(4.3) to

$$\frac{1}{q(z)} = -j\frac{1}{z_{r1}} \tag{4.6}$$

where

$$z_{r1} = \frac{\pi w_{0p}^2 \cdot}{\lambda} \tag{4.7}$$

We will let $q_2(z)$ represent the focal point of the beam after it has been transformed by the back cavity mirror. The pump and transformed beam waists are represented by w_{0p} and w_{0t} respectively.

If we invert Eq.(4.5) and make the substitution for $q(z)$ we have

$$\frac{1}{q_2(z)} = \frac{jCz_{r1} + D}{jAz_{r1} + B}. \tag{4.8}$$

We can extract the transformed beam radius from the imaginary part of Eq.(4.8) and plot this versus the cavity waist size as a function of the separation of the cavity mirrors, we are helped here becasue the real part of Eq.(4.8) is equal to zero. This will provide us with the positions of the cavity mirrors with respect to the focusing lens.

The ray matrix for the optical train is obtained by multiplying the matrices for each element in the beam path in reverse order. Figure 4.9 shows the individual matrices and their respective elements. M_1 represents the distance between the pump waist after the focusing lens—this will be a negative distance—and the planar surface of the back cavity mirror, M_2 represents the matrix for the back cavity lens/mirror and M_3 represents the
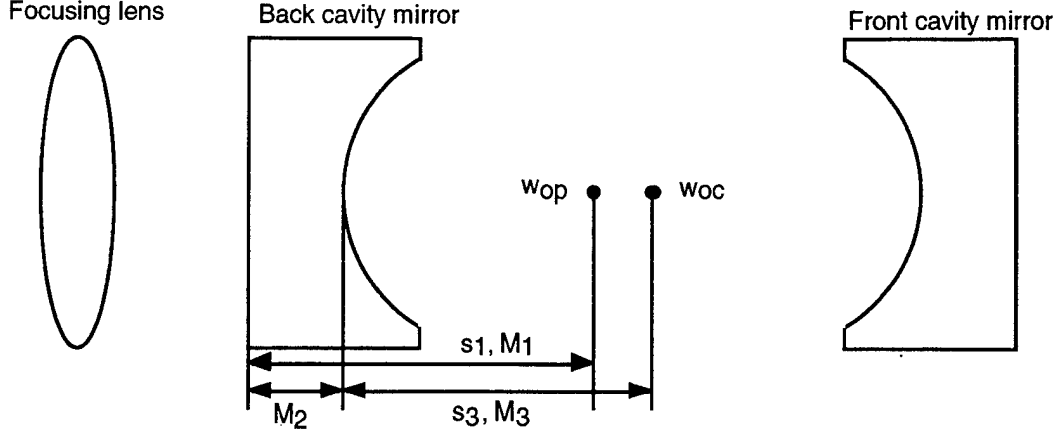
20

Figure 4.9: Ray tracing matrices for determining the cavity mirror positions.

distance between the cavity waist and the curved surface of the cavity mirror. The cavity mirrors are transmissive at the pump wavelength and highly reflective at the signal and idler wavelengths. The matrices for M_1, M_2 and M_3 are

$$M_1 = \begin{bmatrix} 1 & s_1 \\ 0 & 1 \end{bmatrix}, \tag{4.9}$$

$$M_2 = \begin{bmatrix} 1 & \frac{t_c}{n} \\ \frac{1-n}{-R} & \frac{1-n}{-R}\frac{t_c}{n} + 1 \end{bmatrix}, \text{and} \tag{4.10}$$

$$M_3 = \begin{bmatrix} 1 & s_3 \\ 0 & 1 \end{bmatrix}, \tag{4.11}$$

where t_c is the center thickness and R is the radius of curvature of the cavity mirror. The composite matrix for the system is found by multiplying the individual matrices in reverse order of occurrence in the beam path:

$$M_{total} = M_3 M_2 M_1. \tag{4.12}$$

For simplicity, let us refer to the matrix elements of M_2 as A_2, B_2, C_2 and D_2. Thus, Eq.(4.12) becomes

$$M_{total} = \begin{bmatrix} A_2 + C_2 s_3 & A_2 s_1 + B_2 + C_2 s_1 s_3 + D_2 s_3 \\ C_2 & C_2 s_1 + D_2 \end{bmatrix}. \tag{4.13}$$

If we substitute the matrix elements of M_{total} into Eq.(4.8), we obtain

$$\frac{1}{q_2(z)} = \frac{jC_2 z_{r1} + C_2 s_1 + D_2}{j\left(A_2 + C_2 s_3\right)z_{r1} + A_2 s_1 + C_2 s_1 s_3 + B_2 + D_2 s_3}. \tag{4.14}$$

21

We can find the transformed beam waist at the focal point by recognizing that

$$\frac{1}{q_2} = \frac{1}{R(z)} - j\frac{\lambda}{\pi w_{0t}^2}.$$ (4.15)

We can equate the imaginary parts of Eqs.(4.8) and (4.15) and solve for w_{0t}, providing us with

$$w_{0t}(s_1, s_3) = \sqrt{\frac{\lambda}{\pi} \frac{\left((A_2 + C_2 s_3)(C_2 s_1 + D_2) - (A_2 s_1 + C_2 s_1 s_3 + B_2 D_2)C_2\right)z_{R1}}{(C_2 s_1 + D_2)^2 + C_2^2 z_{R1}^2}}.$$ (4.16)

Note that Eq.(4.16) is a function of s_1 and s_3. We need to establish the relationship between these two distances. To do this, we will solve for s_3 in terms of s_1. This can be done by recognizing that the real part of Eq.(4.8) must be equal to zero, since we are analyzing the transformed beam at its waist. We then have

$$s_3(s_1) = \frac{A_2 C_2 z_{R1}^2 + (A_2 D_2 + B_2 C_2)s_1 + A_2 C_2 s_1^2 + B_2 D_2}{C_2^2 z_{R1}^2 + C_2^2 s_1^2 + 2C_2 D_2 s_1 + D_2^2}.$$ (4.17)

The last step is to plot Eq.(4.16) and the OPO cavity mode waist versus s_1—keep in mind that this is a negative distance. The cavity mode waist is

$$w_{0c}(s_3(s_1)) = \left[\frac{s_3(s_1)}{\pi}\sqrt{\frac{1 + g(s_3)}{1 - g(s_3)}}\right]^{0.5}$$ (4.18)

where

$$g(s_3) = 1 - \frac{2s_3}{R}.$$ (4.19)

and R is the radius of curvature of the cavity mirror. Find the distance, s_1, at which w_{0t} and w_{0c} intersect and calculate $s_3(s_1)$. If w_{0t} and w_{0c} do not intersect there are several options: a more tightly focusing lens can be used; the MOPA beam can be expanded and recollimated; or the radius of curvature of the cavity mirrors can be increased. A sample Mathcad program of the mode matching calculations is included in Appendix B.

It is also important to check that s_3 is physically realizable given the space required for the PPLN and oven assembly. To determine the cavity spacing we cannot simply multiply s_3 by 2. We must consider the effective cavity length that results from the insertion of the PPLN. Recall that the index of refraction of lithium niobate is 2.165. Because we have designed a compact system, the PPLN will occupy approximately half the cavity and the optical beam will see a cavity that is 'shorter' than the optimum spacing. To account for this the cavity spacing is determined using the relation

$$L_{cavity} = 2s_3 + L_{PPLN}\left[1 - \frac{1}{n_{PPLN}}\right].$$ (4.20)

L_{cavity} must be greater than the width of the oven assembly.

4.5.3 Physical Alignment of the OPO Cavity

The mode-matching calculations in the previous section will determine the gross positions of the cavity elements. However, due to the inherent margins of error in the beam measurement and a train of optical elements that each impart slight influences on beam shape and focal point, it is necessary to rely on interferometric patterns to fine tune the alignment of the cavity. For this next process, an infrared viewing device, variable aperture and shearing plate are needed.

The placement of the cavity elements begins with aligning the back cavity mirror such that the reflection of the pump laser propagates collinearly with the forward beam. To do this, place the back cavity mirror in position as determined by Eq.(4.20), insert the variable aperture between the focusing lens and the turning mirror, and set the aperture diameter to match the diameter of the beam. When the back cavity mirror (BCM) is perfectly aligned, its reflection will be approximately the same size as the aperture and will pass through it.

Turn the MOPA on to low power and set the aperture to approximately the width of the pump beam. When first placed, the BCM will most likely not be well aligned and its reflection can be just about anywhere. Find the reflection with a small IR viewing card and walk the beam over to the aperture. If the reflection is noticeably larger or smaller than the aperture, the source of the discrepancy must be found. Recheck all calculations and placement of the BCM to find the error. Now, look at the transmitted pump beam some distance from the BCM. It is important that it remain at the height and horizontal center chosen for the beam path. If the deviation is large—more than a millimeter—adjust the turning mirror, the BCM and the focusing lens until the beam is simultaneously aligned in the forward and backward directions.

The front cavity mirror (FCM) is the next element to be aligned. Place it in its appropriate position and align it similarly to the BCM. Its reflection will be slightly larger than the reflection of the BCM since the PPLN has not yet been placed inside the cavity—remember this will modify the radius of curvature of the wavefront at the mirrors. The shape, brightness and character of the reflections on the aperture carry much information about the possible misalignment of the mirrors. It is well worth the effort to spend a day changing the positions of the mirrors and lens, observing the small differences in beam that each contributes. This will enhance the experimenter's understanding of the dynamics of the cavity and will reduce the possibility of misalignment due to a malperceived visual cue. This point cannot be stressed enough.

The rest of the mode-matching alignment must be done with the PPLN in the OPO cavity. Let us label the direction of propagation through the OPO system the z-axis, the vertical direction the y-axis and the horizontal direction the x-axis—with a right hand orientation. The placement of the PPLN along the y- and z-axes is not critical, as long as the crystal is reasonably centered. However, the placement in the x direction is somewhat more complicated. The PPLN must be placed such that it is as nearly perpendicular to the z-axis as possible and the pump beam should pass through the centers of the 500 μm wide crystal end faces. This is not an easy thing to verify directly since the cavity is only a few millimeters wider than the PPLN oven mount, making it impossible to view the beam as it enters the crystal face. I used an IR CCD camera and looked at both the exit face and the side view of the crystal as it was moved into and out of the beam path. This provided

me with very little usable information due to the extreme sensitivity of the CCD camera to IR light. A small amount of scattered light was always present and masked the forward propagating beam.

The method of alignment that worked the best utilized the second harmonic properties of the PPLN. The period of the PPLN grating in our experiments is 28.5 μm. The periodicity of a grating for second harmonic generation is approximately 5.5 μm. Thus the 979.5 nm pump will produce a small amount of blue light at 489 nm from a 5th order effect of the grating. The alignment process is now very simple. Operate the MOPA at moderate power and view the transmitted beam of the cavity without the PPLN in place. Next move the PPLN slowly through the beam until a round spot again appears on the IR viewing card. Turn the MOPA power up to 750 mWatts, darken the room and look for blue light from the cavity. A white card works well for this. Slowly move the PPLN until a single round spot of blue is apparent. Now, if the PPLN is slightly rotated about the z-axis, the blue beam will be visible on the crystal faces when the crystal is not perpendicular to the pump. Gently rotate the PPLN until the reflection of the blue light is at a minimum on each face and the transmitted portion is bright and well formed. Recall that the phase-matching conditions are highly dependent on temperature. Therefore the PPLN must be near its predicted temperature for the alignment procedure. If the blue is so faint that it is nearly impossible to see, change the oven temperature by a degree or two and the blue should become brighter.

When the cavity is mode-matched, the interference pattern of the reflections from the cavity mirrors will be in the form of a straight line interferogram. To view the interferogram, place a thin wedge in the beam path—a microscope cover slip or pellicle works well—and view the interference pattern on a card with the IR camera. The pattern should show distinct curved lines when the cavity is empty. Next, place the PPLN inside the cavity and center the beam on the crystal face as described above. As the crystal is moved into place, the rings should straighten out if the cavity is close to proper alignment. The next step is to slowly move the cavity mirrors closer or further apart and look for a change in the straightness of the interference lines. The point at which the lines seem straightest is probably the best alignment position. Finally, place the detectors and appropriate filters in the beam path and look for OPO activity. It may be necessary to gently tweak the mirrors until the resonant positions are found.

5 CW DPOPO MECHANICAL DESIGN

5.1 OPO Housing

The mechanical housing of the OPO was designed to minimize fluctuations in the optical pathlength. We chose to manufacture the main frame of the housing of the OPO from an eight inch extruded aluminum box (Fig. 5.1 shows an external view of the housing). One side of the box was removed leaving a U-shaped frame that forms the base and sides of the housing. A plexiglass sheet provides a see-through cover for the device. This monolithic design provides better stability and stiffness than separately machined components. We then cut plates from the same extrusion to enclose the ends of the housing. Prior to assembly, the aluminum housing was annealed at 350 °C for three hours to relieve stress that may have

been present in the metal. Mechanical drawings for the housing components and mounts are included in Appendix C.

The optical components of the OPO are bolted directly onto the aluminum housing. The height of the optical path is 2 inches from the top of the housing floor and four inches from the surface or table that the housing rests upon. The low profile was chosen to accomodate standard optical risers for use in experiments requiring an optical table. The housing mounts directly to a table via three 1/4" clearance holes in the horizontal feet of the end plates. Three point contact is made to minimize deformation of the base when clamped to a rigid surface. All cables into the housing are strain relieved by the exhaust vent cover. Removal of the vent cover provides access to the strain relief slots.

5.2 Device Layout and Component Attachment

Figure 5.2 is a photograph of the layout of the OPO prototype. The SDL MOPA is attached to the OPO base through four side clamps that fit into a horizontal slot along the base of the MOPA housing. The MOPA rests on two pins that fit into milled slots in the bottom of the base. This design ensures proper alignment and stress relief, and allows easy removal and insertion of the MOPA. The diode laser in the MOPA is attached to a thermo-electric cooler which is bonded to the base of the MOPA housing. Cooling for the TE cooler is provided by a small fan attached to the end of the laser. The end plate of the OPO housing was machined with a 1.5 inch hole to allow air passage to the fan (Fig. 5.3).

The pump beam is horizontally polarized as it exits the MOPA housing. It passes through an Isowave optical faraday isolator (Isowave Model No. I-98T-5M) to prevent backward propagating waves from interfering with the coherency of the laser. The polarization of the pump beam is rotated 45 ° by the isolator. The pump beam is then turned 180 ° by two aluminum turning mirrors, and rotated back to a horizontal polarization by a $\lambda/2$ plate. It passes through a focusing lens, back cavity mirror, PPLN crystal, and front output coupler and is absorbed in the end plate via a BG-38 filter. The 1.96μm light generated by the OPO freely outcouples from the housing through the filter.

5.3 PPLN Crystal Oven

The crystal oven was designed to minimize mechanical strain on the lithium niobate crystal, and to maintain a uniform temperature throughout the crystal (Fig. 5.5). Due to its strong piezo-electric properties, the nonlinear coefficient of PPLN can be locally altered by an external pressure. Thus it is unwise to clamp the crystal to a hard base. We chose to orient the PPLN crystal vertically in the cavity, with the extraordinary axis oriented horizontally. The crystal rests against a thin piece of alumina that was epoxied to a solid copper base. The crystal is held in place by fitting the bottom edge into a small wedge created by attaching a 2 mm glass rod to the copper block. The top of the crystal is securely, but gently anchored by a small piece of spring steel that contacts the exposed top edge of the crystal at a 45° angle thus imparting equal forces, seating the crystal down into the wedge and against the flat alumina surface. The oven was fabricated from solid copper for efficient thermal conductivity and is resistively heated by a 50 Ω resistor. A constant temperature is maintained by monitoring the oven temperature with a thermistor by a resistive heater controller module from Wavelength
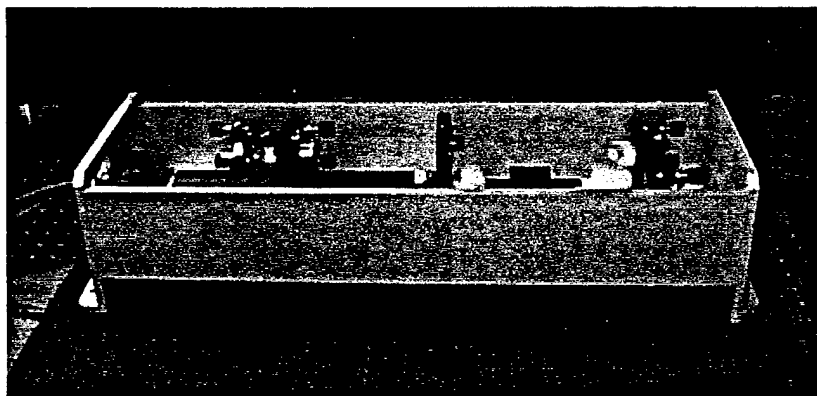
Figure 5.1: Photograph showing an external view of the OPO housing.
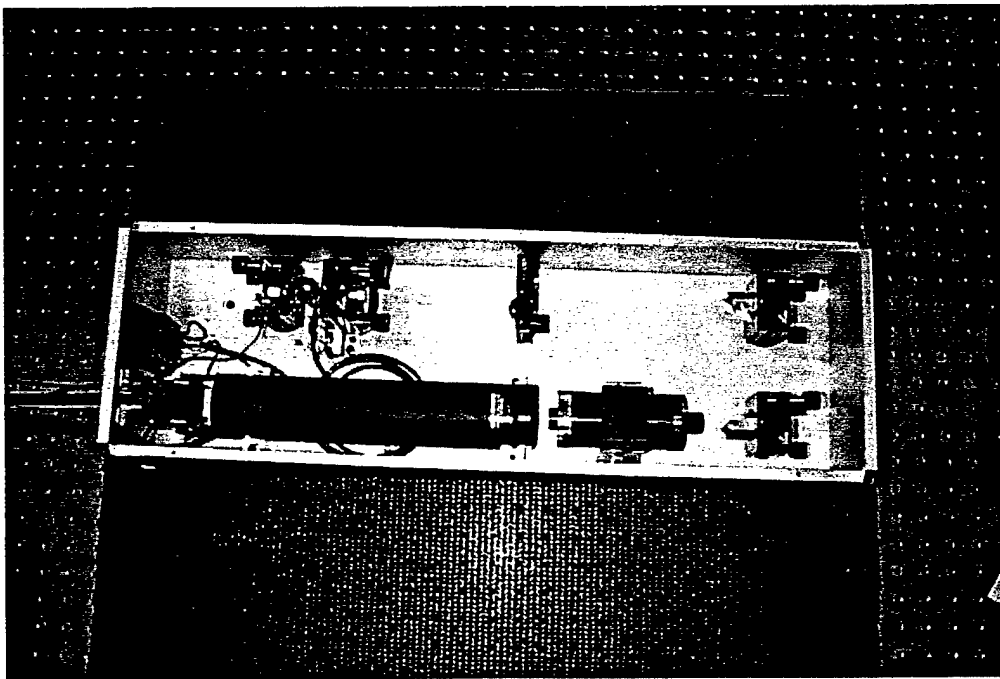
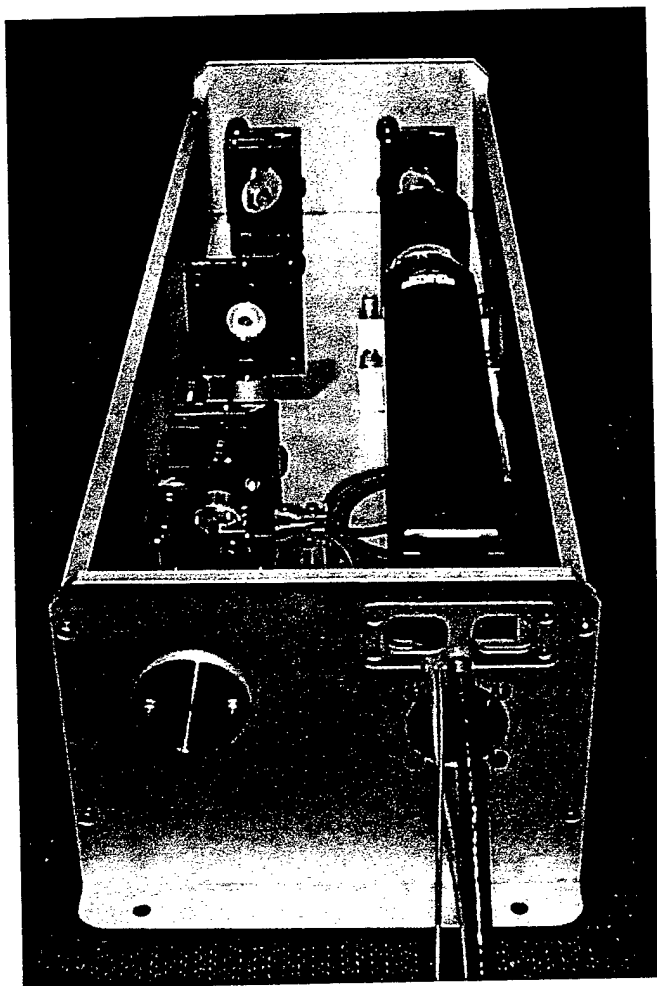Figure 5.2: Photograph of the inside of the OPO prototype.

Figure 5.3: Photograph of the end plate of the OPO housing showing the vent slots and fan.

Electronics (Fig. 5.4). The RHM-4000 is attached to the front end plate of the housing and is powered by placing a 24 volt potential between the terminals of the green cable. The yellow lead is positive and the green lead is negative (or ground).

The oven assembly can be translated vertically, and transverse to the optical path. Rotation about the axis perpendicular to the base of the housing is effected by a nylon screw that attaches the oven to the base of its mount. Horizontal and vertical translation are made by adjusting the spline head set-screws on the oven mount translation stages. Spline wrenches are included with the housing.

5.4   Operating the SDL MOPA

The SDL MOPA is most effectively and safely driven by the ILX LDC-3900 Modular Laser Diode Controller. The MOPA has three components that are driven separately and require careful monitoring of current, voltage and temperature. The ILX driver has four ports for integrating modules that are designed specifically to safely operate the SDL MOPA. The TCM-39032 is a 32 watt thermo-electric cooler module that maintains a TEC temperature between its rated operating points to with ± 0.0001 °C. The CSM-39400M 4 Amp Current Source Module is the appropriate unit for driving the amplifier of the MOPA. It can deliver up to 4 amps of current at the correct diode voltage. The CSM-39020 200 mA Current Source Module has a 200 mA maximum output current and is used to drive the laser oscillator in the MOPA. The ILX unit has error condition shutoff control circuitry that detects when over voltage, over current or over power limits are reached. The unit safely shuts power to the lasers and displays the corresponding error message on the front panel. This type of circuit protection is critical when operating high-powered and expensive diode lasers.

5.5   Operation of the Queensgate Piezo-electric Stage

The front cavity mirror/output coupler is mounted on a piezo-electric actuator that has a 20 μm range of translation. The piezo stage is used to scan the output coupler to a point where the OPO cavity is resonant for both the signal and idler waves. The piezo stage is driven by a Queensgate driver that has an output range of 10–150 volts. The driver can be used directly to drive the piezo stage, or a specific waveform can be generated by a function generator and fed into the driver. We applied a triangle wave to the driver and monitored the output to the piezo stage on an oscilloscope. The piezo motion can only be monitored if the Queensgate is externally driven by a waveform generator.

6   CONCLUSION

Cygnus Laser has demonstrated that a CW DPOPO is a physically realizable device when pumped with a stable diode laser. We consider the work performed under this contract to be technically important to the scientific community. This work has contributed to the understanding and further development of a compact and tunable mid-infrared laser based source. The problems encountered with the SDL MOPA prevented Cygnus Laser from delivering a working unit to Phillips Laboratory. However, the work performed under this

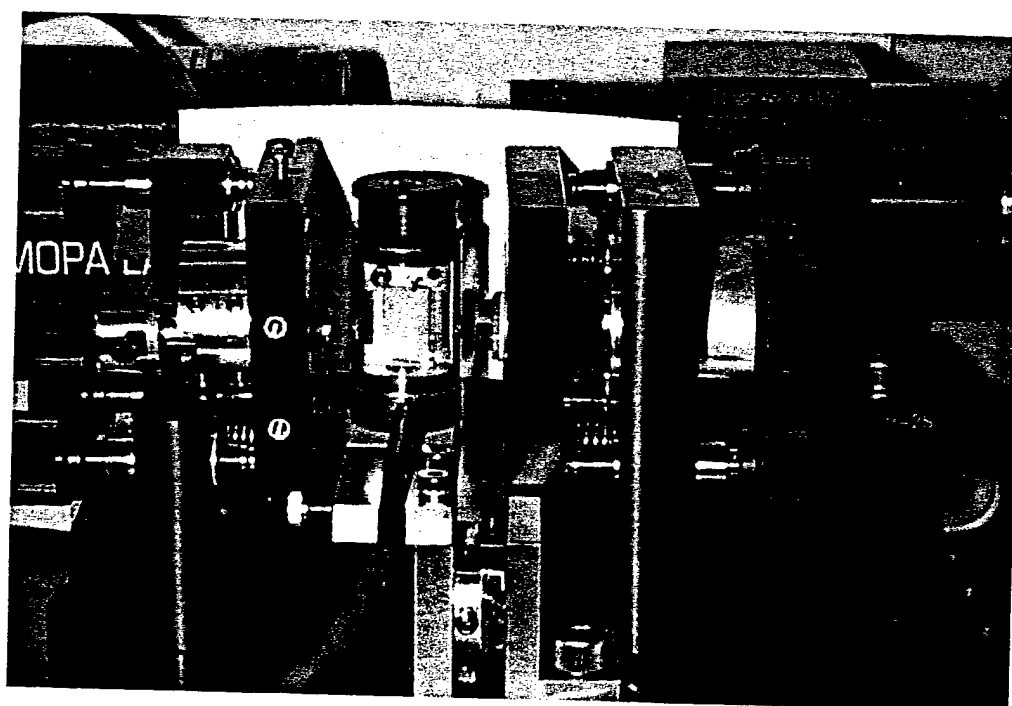Figure 5.4: Photograph of the Wavelength Electronics temperature controller.

Figure 5.5: Photograph of the PPLN oven.

contract has brought the technology to a point where the identification and demonstration of a high-powered diode laser that meets the mode stability and beam characteristics of our system is all that is needed to realize a working CW DPOPO.

References

[1] D. Eimerl, IEEE J. Quantum Electron. **QE–23**, 575 (1987); "High Average Power Harmonic Generation."

[2] D. Eimerl, IEEE J. Quantum Electron. **QE–23**, 1361 (1987); "Quadrature Frequency Conversion." There is a nontrivial typographical error in Eimerl's expression for η_{max}: in his notation, this paper lists

$$\eta_m \equiv \frac{(1 + f_2)F}{t_1^2(F + G)};$$

the correct definition is

$$\eta_m \equiv \frac{(1 + f_2)G}{f_2 t_1^2(F + G)}.$$

[3] G. D. Boyd and D. A. Kleinman, J. Appl. Phys. **39**, 3597; "Parametric interaction of focused Gaussian light beams."

[4] J. A. Armstrong, N. Bloembergen, J. Ducuing, P. S. Pershan: Phys. Rev. **127**, 1918, (1962).

[5] J. A. Giordmaine and R. D. Miller, Appl. Phys. Lett. **9**, p. 298 (1966).

A APPENDIX A
STANFORD FINAL TECHNICAL REPORT

Electric-field-repoled lithium niobate for diode-laser-pumped optical parametric oscillation

Final Technical Report
Cygnus Laser Subcontract CLC-SUB-DSH-94-001
Air Force Phillips Laboratory Prime Contract F29601-94-C-0144
August 1, 1994 through September 30, 1995

Robert L. Byer
Principal Investigator

Edward L. Ginzton Laboratory
Stanford University
Stanford, California 94305-4085

Electric-field-repoled lithium niobate for diode-laser-pumped optical parametric oscillation

Cygnus Laser Subcontract CLC-SUB-DSH-94-001
Final Technical Report

Robert L. Byer
Edward L. Ginzton Laboratory
Stanford University
Stanford, California 94305-4085

ABSTRACT

We have used periodically poled LiNbO$_3$ (PPLN) prepared by patterned electric-field poling as a nonlinear optical material for direct semiconductor-diode-laser pumping of an optical parametric oscillator (OPO). This program built upon earlier investigations that resulted in development of techniques for the reliable processing of this material. During this investigation we have extended material processing techniques to reliably produce larger samples up to several cm in length. PPLN used for quasi-phase-matched (QPM) nonlinear parametric interactions provides advantages over conventional birefringent phase matching such as larger effective nonlinearity permitted by accessing d_{33} component of the nonlinear tensor and the avoidance of birefringent walkoff. The large effective nonlinearity and noncritical phase matching available with PPLN were important factors in the success of this program.

The body of this report was reproduced with permission from the Ph.D. dissertation of L. E. Myers.

35

Electric-field-repoled lithium niobate for diode-laser-pumped optical parametric oscillation

Cygnus Laser Subcontract CLC-SUB-DSH-94-001
Final Technical Report

Table of Contents

36

Electric-field-repoled lithium niobate for diode-laser-pumped optical parametric oscillation

Cygnus Laser Subcontract CLC-SUB-DSH-94-001
Final Technical Report

Personnel Associated with the Program

Robert L. Byer	Principal Investigator, Professor of Applied Physics
Martin M. Fejer	Associate Professor (Research) of Applied Physics
Robert C. Eckardt	Senior Research Associate Ginzton Laboratory
Lawrence E. Myers	Graduate Student, Ph.D. 1995 Electrical Engineering
Robert Batchko	Graduate Student Applied Physics

Electric-field-repoled lithium niobate for
diode-laser-pumped optical parametric oscillation

Robert L. Byer
Principal Investigator

For doubly resonant oscillators (DRO's) in periodically poled lithium niobate (PPLN), calculations predict thresholds readily within range of commercially available cw diode lasers. An OPO directly pumped by a diode laser is especially interesting as a compact and efficient source of tunable radiation. Other approaches to building diode-pumped OPO's using available nonlinear optical materials have been hampered because the gain and phasematching conditions place difficult constraints on the wavelength and power requirements of the pump laser[1,2]. With the engineerable phasematching and high gain properties available through quasi-phasematching, we demonstrated an OPO directly pumped by a commercial cw diode laser.[3,4]

In preparation for direct diode pumping, we built a DRO pumped by a Ti:sapphire laser using the PPLN crystal described in the next section. We used 2 HR mirrors at the signal wavelength similar to those described in the next section except that they had 25-mm radius of curvature which required spacing with near spherical separation to produce the desired mode waist in the crystal. We tried pumping with the Ti:sapphire laser before the diode laser because of its good beam quality and single frequency operation. However, we were forced to operate no longer than ~970 nm because of the limited gain of the Ti:sapphire laser. This caused the phasematching relative to our design wavelength of 977 nm (see Fig. 1) to be very close to the degeneracy point at room temperature. We obtained oscillation with pump wavelengths from 968-972 nm at room temperature. The minimum oscillation threshold was 105 mW for λ_p=969 nm. This value was higher than the predicted value of <40 mW due to problems with aligning the long cavity and pump with a wavelength on the margin of the phasematching. However the results proved that threshold powers achievable with diode lasers could be obtained using the available PPLN crystals.
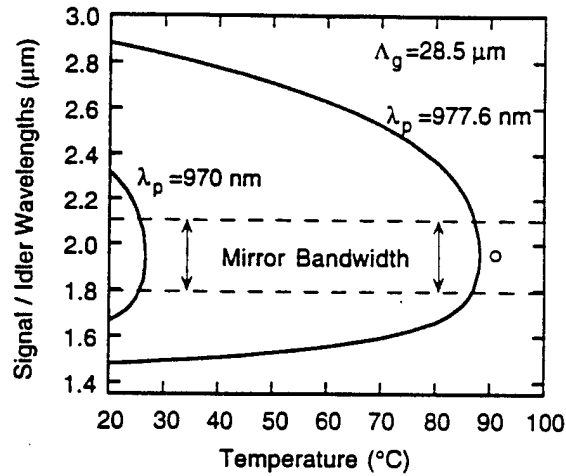
38

Fig. 1. Calculated temperature tuning curve for 28.5-μm period PPLN OPO. Calculated phasematching temperature for λ_p=977.6 nm at degeneracy is 88 °C; experimental measurement is 91 °C. The bandwidth of the mirrors used in the experiments is indicated.

Diode Pump Laser and Experimental Set-Up

The pump was a 977.6-nm master oscillator/power amplifier (MOPA) diode laser from SDL, Inc. (model 5762). The laser was found to have reliable single frequency operation at limited points over its operating range of amplifier current and temperature. The laser was rated for 750 mW, but we operated at 500 mW for better stability. We used a scanning confocal interferometer and etalons to verify single frequency operation of the

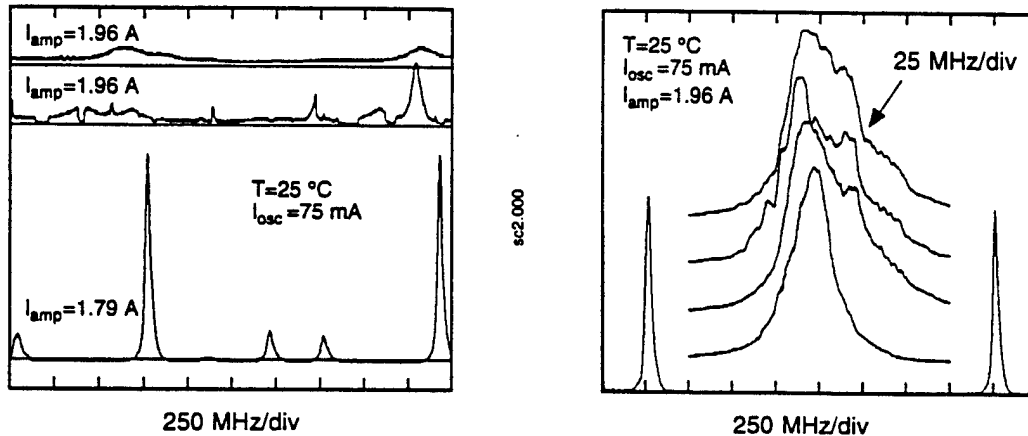

Fig. 2. Output of scanning confocal interferometer for the MOPA diode laser. All traces have same vertical scale with offsets shifted for clarity. (a) Examples of multi-mode and broad band output for nearby settings of amplifier current. (b) Examples of single frequency output. The insets show 10x expansion of peak. The linewidth of ~25 MHz is comparable to the measurement resolution.

39

diode laser. The laser had regions of single frequency (line width ~25 MHz), multi-mode, and broad band (line width >7 GHz) behavior depending on the amplifier current and temperature settings, as shown in Fig. 2. The laser was susceptible to even small amounts of feedback; -60 dB of isolation was required for stable operation.

The experimental set-up of the diode-pumped OPO is shown in Fig. 3. The doubly resonant OPO resonator was a linear cavity with 10-mm radius of curvature mirrors separated by 22 mm. We used a high reflectivity input mirror and output couplers of 0.3% and 0.7% transmission all centered at 1.96 μm. The useful bandwidth of the mirrors was about 200 nm, and the pump reflectivity was ~20% for each mirror. The pump beam was focused to a 33-μm waist in the cavity with a beam quality of M^2=1.3. The beam had an ellipticity of 1.2 and astigmatism of 2.5 mm in the focus locations in air. The output coupler was mounted on an annular piezoelectric element for cavity length control. The OPO output near 1.96 μm was detected with a PbS detector after a filter that blocked the pump beam, while the transmitted pump beam was detected with a Si detector.

The PPLN crystal for the diode-pumped OPO was 0.5-mm thick with a 9.3-mm interaction length. The domain period for quasi-phasematching was 28.5 μm, designed for degenerate operation at 88°C as shown in Fig. 1. The polished end faces of the PPLN were AR coated for the signal/idler pair near degeneracy. The total single-pass power loss through the two coated surfaces and the crystal was 0.8%. The peak phasematching temperature was measured at 91°C which agrees with the design calculation.
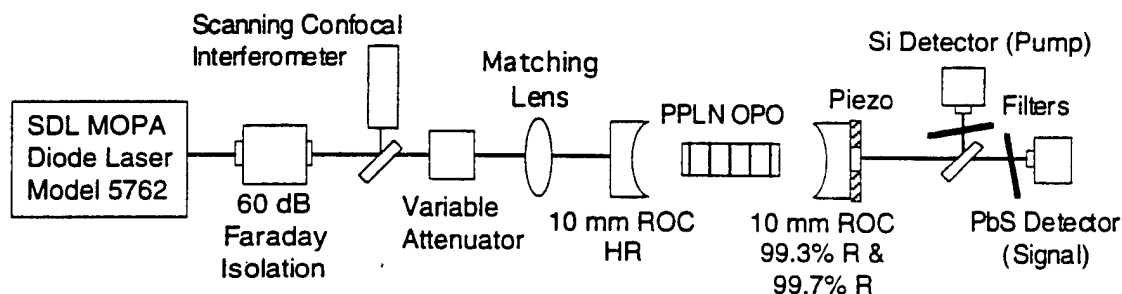

Fig. 3. Experimental set-up for diode-pumped OPO in bulk PPLN.

40

DRO Threshold

The threshold for a DRO is given by[5,6]:

$$P_{th} = \frac{a_s a_i}{4\eta_d} \frac{n_s n_i c^4 \varepsilon_0 \pi}{\omega_s \omega_i \omega_p d_Q^2 L \bar{h}_m} \tag{1}$$

where $\bar{h}_m$ is the Boyd and Kleinman reduction factor for a focused interaction, L is the crystal interaction length, ω_p, ω_s, and ω_i are the pump, signal, and idler frequencies, and n_s, n_i, a_s, and a_i are the refractive indices and round trip power losses of the signal and idler respectively. The nonlinear coefficient adjusted with constant Miller delta is $d_Q = (2/\pi)d_{33} = 14.7$ pm/V. The round trip power losses were 1.9% and 2.3% for the 0.3% and 0.7% output couplers respectively. Minimum threshold is attained when $L/b = 2.8$ and $\bar{h}_m = 1.07$. In our case, $\bar{h}_m \approx L/b = 0.62$ (the waists are $w_{0p} = 33$ μm and $w_{0s} = 47$ μm). The predicted threshold power was 43-50 mW for the 0.3% output coupler and 62-72 mW for the 0.7% output coupler, where the range of values covers the ideal efficiency $\eta_d = 1$ and de-rating $\eta_d = 0.86$ for duty cycle errors of the PPLN. The measured thresholds were 61 mW and 98 mW for the 0.3% and 0.7% output couplers, respectively.

Fig. 4 shows the cavity mirror piezo voltage, pump transmission through the cavity, and the OPO output through a 0.7% output coupler as the cavity length is scanned with the piezo. The OPO output could be shifted relative to the pump transmission by adjusting the temperature and the cavity length. The plot on the left of Fig. 4 shows a case

20 ms/div   20 ms/div

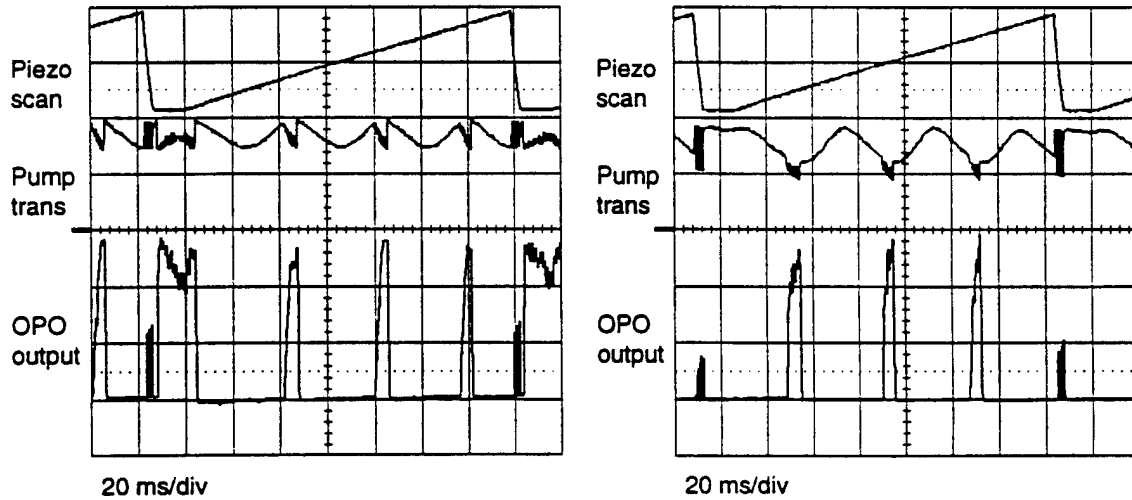**Fig. 4.** Cavity mirror piezo scan voltage, pump transmission with depletion, and ~1.96-μm OPO output signals with 0.7% output coupler. The left plot shows an operating point near the peak of the pump transmission. The right plot shows a different operating point near the minimum of the pump transmission.

41

where the output occurs near a peak of the pump transmission, while the plot on the right shows a different operating point where the OPO output occurs near a pump transmission minimum. The 20% reflectivity of the cavity mirrors at the pump wavelength formed a cavity with finesse of 1.7 (neglecting the weak etalon of the crystal surfaces), so the circulating pump intensity could range from 0.5 to 1.2 times the incident power. Even a low finesse cavity such as this can produce noticeable etalon effects, but the fact that the OPO oscillated during the pump transmission minimum indicates that threshold was reached without pump enhancement.

4.3.3. Conversion Efficiency and Stability

The theoretical conversion efficiency is given by[5]

$$\frac{P_s + P_i}{P_p} = 2\frac{T_{OC}}{T_{OC} + a_D}\frac{\sqrt{N} - 1}{N} \tag{2}$$

where T_{OC} is the transmission of the output coupler, a_D is the losses in the crystal and the other cavity mirror, and N is the number of times above threshold. This expression for the plane wave case can be shown to also apply to mode-matched focused Gaussian beams.[7] Using our measured threshold values gives predicted efficiencies of 13% and 23% for the 0.3% and 0.7% output couplers respectively. For 370 mW of pump incident on the cavity mirror, we measured peak output powers of 34 mW and 64 mW with 0.3% and 0.7% output couplers respectively. These values were determined by measuring the average power in the output beam and adjusting for the duty factor of the actual OPO operating time over the piezo scan. The conversion efficiencies of 9% and 17% agree reasonably well with the predictions and with the values obtained from pump depletion as shown in Fig. 4.

Note in Fig. 4. where the piezo position was held at a resonant point for the OPO during the flat part before the voltage ramp. Figure 5 shows a case with the piezo ramp slowed down to emphasize the cw operation. The relatively stable nature of the output indicates the potential for adding control electronics to make a useful cw infrared tunable source.
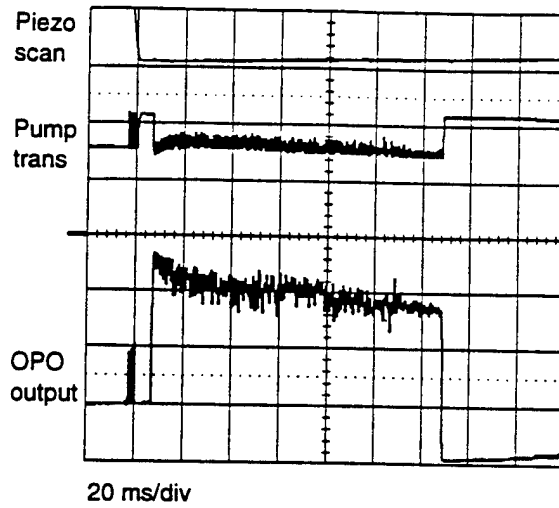
Fig. 5. CW operation with piezo held nearly stationary, showing the potential for stabilizing the output.

4.3.4. DRO Cluster Effects

The OPO runs in disjoint regions as a function of cavity mirror separation due to the cluster effect that is well-known for DROs.[8] In general, the cavity mode spacing of the signal and idler are not the same due to dispersion in the nonlinear optical crystal. A cluster occurs when the cavity modes of the signal and idler are simultaneously in resonance. Clusters can be described by the sum of the axial mode numbers of the signal and idler[9]

$$m = m_s + m_i \tag{3}$$

where

$$m_{s,i} = \frac{2L + 2l(n_{s,i} - 1)}{\lambda_{s,i}} = \frac{[L + (n_{s,i} - 1)l]\omega_{s,i}}{\pi c}$$

and L and l are the cavity length and crystal length respectively. The cluster spacing as a function of change in cavity length is

$$\frac{\partial m}{\partial L} = \frac{\omega_s + \omega_i}{\pi c} = \frac{\omega_p}{\pi c} \tag{4}$$

As seen in Fig. 4, the cluster spacing is exactly the same as the spacing of the pump resonances. This can be shown analytically from the pump resonance condition, an analogous expression to $m_{i,s}$ in Eq. (3), so the pump resonance spacing as a function of change in cavity length is

$$\frac{\partial m_p}{\partial L} = \frac{\omega_p}{\pi c} \tag{5}$$
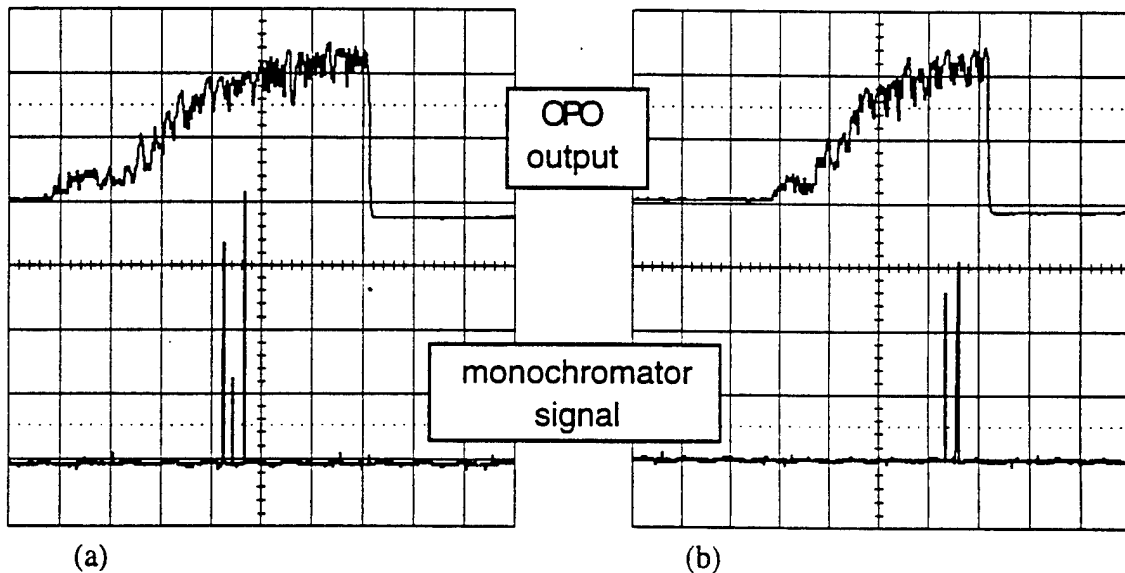
which is identical to Eq. (4).

43

Tuning and Spectral Properties

We monitored the spectral content of the OPO output using a 1-m monochromator. For different wavelength settings, we observed the monochromator output while the cavity mirror was scanned. Typical traces showing the output for a given monochromator setting are shown in Fig. 6. The output spectrum is erratic owing to lack of cavity stabilization which permitted competition between different signal/idler mode pairs within a cluster. However, the centroid of the monochromator output showed a clear dependence on the cavity mirror separation, which is plotted in Fig. 7. With mirror translation of ~50 nm, signal/idler pairs were observed from 1.85-2.08 μm which is the extent of the mirror bandwidths.

Fig. 6. Monochromator output vs. OPO output while the piezo is scanning through one cluster. (a) Monochromator set at 1.890 μm. (b) Monochromator set at 2.000 μm.

As the cavity length is scanned, the output frequencies follow the cavity resonance until they reach degeneracy. There is a subsequent gap in the OPO output until the cavity length changes enough to bring another cluster within the mirror bandwidths. The tuning behavior within a cluster can be described by a Taylor series expansion of the change in cluster number[9]

$$\Delta m = \frac{1}{2}\left(\frac{\partial^2 m}{\partial \omega_s^2}\right)_{\omega_p} \cdot (\omega_s - \omega_0)^2 + \frac{\partial m}{\partial L}\Delta L \equiv 0 \tag{6}$$

(a)   (b)

44

where the derivative in parentheses means the derivative is taken with ω_p held constant. The details of the calculation are given in Appendix C, and the resulting theoretical curve describing the tuning as a function of cavity length change for the conditions of this experiment is shown in Fig. 7. The calculation agrees reasonably well with the measurements. Possible reasons for discrepancy are uncertainty in the calibration of the piezo movement and pulling of the gain by the mirror reflectivities centered at degeneracy.
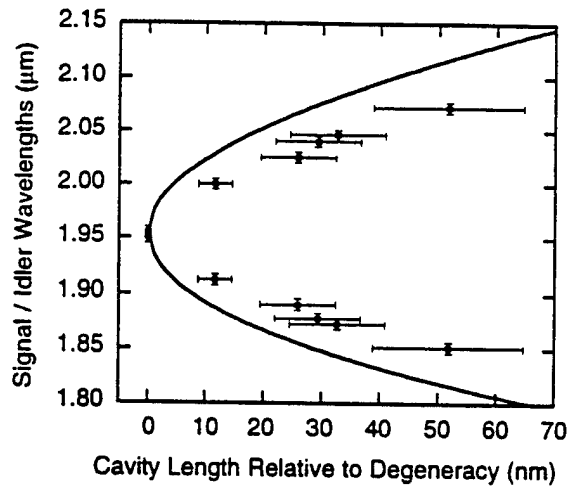

Fig. 7. Centroid of spectral output of the cw-diode-pumped DRO as a function of cavity mirror separation.

Beam Quality

We qualitatively measured the beam quality of the OPO by collimating the beam and observing the spot with an IR vidicon camera. To collimate the beam, we used a lens with the same focal length as the matching lens shown in Fig. 3 placed a comparable distance after the cavity. We used filters to block the pump beam and any other stray light. The pictures in Fig. 8 show that the beam appears to be a TEM_{00} Gaussian mode in profile and propagation. This results from the definition of the OPO spatial mode by the resonant cavity.
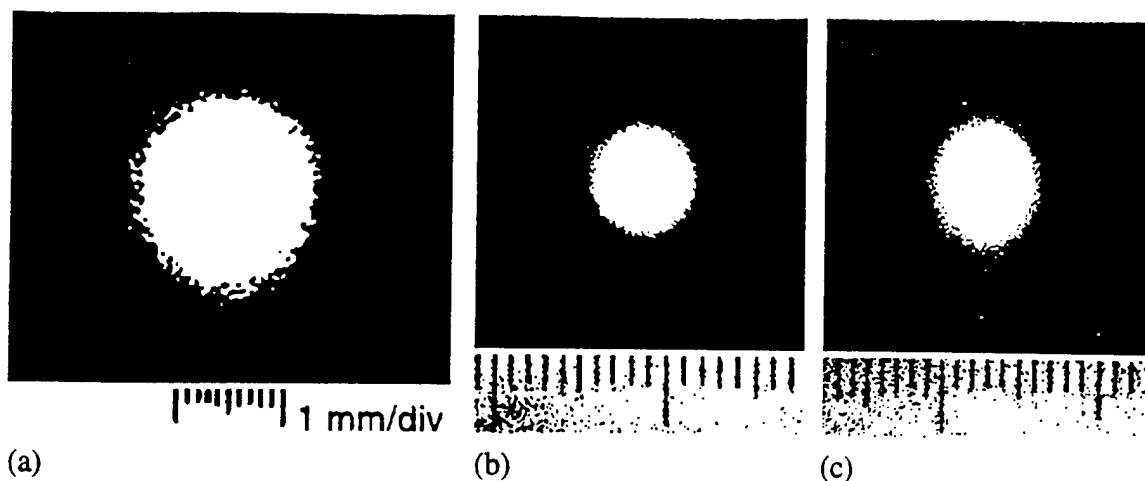
45

(a)   (b)   (c)

Fig. 8. OPO beam viewed with IR vidicon camera. (a) 0.43 m after cavity output coupler, before collimating lens. (b) 0.33 m after collimating lens. (c) 1.14 m after collimating lens.

Summary

In summary, we have demonstrated a cw diode-pumped DRO with PPLN. The high gain and engineerable phasematching properties of PPLN allow tailoring the material to match commercially available diode lasers. By holding the piezo at a resonant point of the OPO, the output could be made to run continuously, indicating the potential for stabilizing the OPO power with servo control of the cavity length. The output spectrum was erratic, but with the addition of vibration and environmental isolation, we expect better spectral behavior. With these improvements, this device has the potential to be a useful cw tunable infrared source. Future work will include non degenerate operation for broader spectral coverage and monolithic construction for better stability.

46

References

1. J. Bartschke, R. Knappe, C. Becher, B. Beier, M. Scheidt, K.-J. Boller, and R. Wallenstein, "Application of injection-locked high power diode laser arrays as pump source for efficient Nd:YAG lasers, green or blue lasers and continuous wave KTP optical parametric oscillators," in *OSA Proceedings on Advanced Solid State Lasers*, **20** (Optical Society of America, Washington, DC, 1994), pp. 340-343.

2. M. Scheidt, B. Beier, R. Knappe, K.-J. Boller, and R. Wallenstein, "Diode-laser-pumped continuous-wave KTP optical parametric oscillator, " *J. Opt. Soc. Am. B* **12**, pp. 2087-2094 (1995).

3. L. E. Myers, R. C. Eckardt, M. M. Fejer, R. L. Byer, and J. W. Pierce, "CW diode-pumped optical parametric oscillator in bulk periodically poled LiNbO3," *Electron. Lett.* **31**, pp. 1869-1870 (1995); reproduced as Appendix I to this report.

4. L. E. Myers, R. C. Eckardt, M. M. Fejer, R. L. Byer, W. R. Bosenberg, and J. W. Pierce, "Quasi-phase-matched optical parametric oscillators in bulk periodically poled LiNbO3," *J. Opt. Soc. Am. B* **12**, pp. 2102-2116 (1995); reproduced as Appendix II to this report.

5. R. L. Byer, "Optical parametric oscillators," in Quantum Electronics: A Treatise, vol. I, part B H. Rabin and C. L. Tang, ed. (Academic, New York, 1975), pp. 587-702.

6. G. D. Boyd and D. A. Kleinman, "Parametric interaction of focused Gaussian light beams," *J. Appl. Phys.* **39**, pp. 3596-3639 (1968).

7. G. Breitenbach, S. Schiller, and J. Mlynek, "81% Conversion efficiency in frequency-stable continuous-wave parametric oscillation," *J. Opt. Soc. Am. B* **12**, pp. 2095-2101 (1995).

8. J. A. Giordmaine and R. C. Miller, "Optical parametric oscillation in the visible spectrum," *Appl. Phys. Lett.* **9**, pp. 298-300 (1966).

9. R. C. Eckardt, C. D. Nabors, W. J. Kozlovsky, and R. L. Byer, "Optical parametric oscillator frequency tuning and control," *J. Opt. Soc. Am.* **9**, pp. 646-667 (1991).

B APPENDIX B
SAMPLE MATHCAD FILES

This program calculates the beam waist radius for measured data.

Experimental steps:

1. Measure the beam using a scanning razor blade at the $1/e^2$ points - 86% and 14%. Do this for both the horizontal and vertical directions.

2. Plot the data and determine to a best approximation where the beam waist is.

$$TOL = 10^{-6}$$

Set up matrices for the measured beam data. z = distance from front of mirrormount point, w = beam radius

These are in units of millimeters.

$z = (5 \quad 10 \quad 15 \quad 20 \quad 25 \quad 30 \quad 35 \quad 40 \quad 45 \quad 50 \quad 55 \quad 60 \quad 65 \quad 70 \quad 75 \quad 80 \quad 85 \quad 90 \quad 95 \quad 100 \quad 105 \quad 110 \quad 115)^T$

$w = (.595 \quad .53 \quad .49 \quad .435 \quad .395 \quad .35 \quad .3 \quad .255 \quad .215 \quad .17 \quad .1275 \quad .0825 \quad .0495 \quad .0118 \quad .0395 \quad .0743 \quad .1325 \quad .1$

Given data: $\lambda = 979.5 \cdot 10^{-6}$ $z_0 = 69.75$

Sample guess value for solve block: $w_0 = 0.030$

Equation for gaussian beam profile:

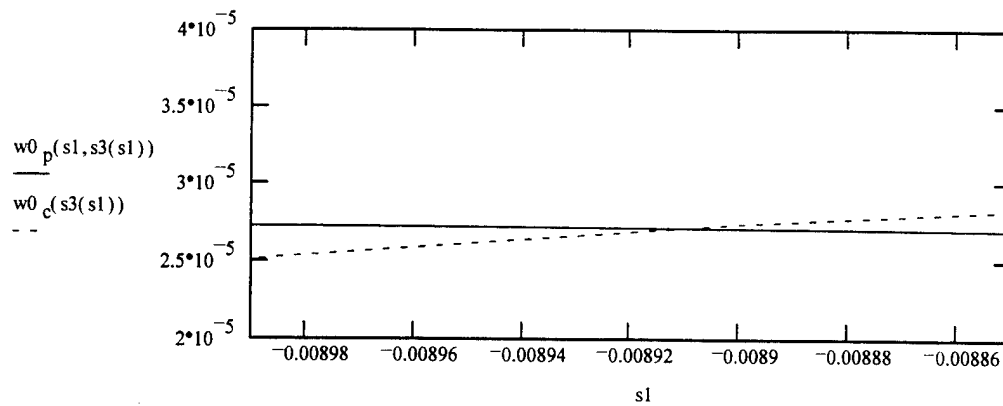$$f(z, z_0, w_0) = w_0 \cdot \sqrt{1 + \left[\frac{\lambda \cdot (z - z_0)}{\pi \cdot w_0^2}\right]^2}$$

Solve block for minerr function.
Given

$$\overline{|w - f(z, z_0, w_0)|} = 0 \quad w_0 > 0 \qquad w_0 = minerr(w_0) \quad w_0 = 0.035$$

Position of Mirror from Input Beam Waist
(neg means mirror is before the waist):
$$s1 = -9 \cdot 10^{-3}, -8.9 \cdot 10^{-3} .. -7.0 \cdot 10^{-3}$$

$$\frac{w0_p(s1, s3(s1))}{w0_c(s3(s1))}$$
$- -$

sl

Match Waist Sizes at same position after the
mirror:

$$s1 = -9 \cdot 10^{-3}$$

GIVEN $w0_c(s3(s1)) \equiv w0_p(s1, s3(s1))$ $S1 = \text{find}(s1)$ $S1 = -8.91 \cdot 10^{-3}$

$S3 = s3(S1)$ $S3 = 9.41 \cdot 10^{-3}$ $w0_c(S3) = 2.713 \cdot 10^{-5}$ $w0_p(S1, S3) = 2.713 \cdot 10^{-5}$

This program calculates the mirror positions for the degenerate OPO cavity with the MOPA diode laser.

<u>Input Cavity Mirror</u>: $TOL \equiv 10^{-6}$

$n = 1.4507$ index of refraction of mirror

$\Phi = 7.75 \cdot 10^{-3}$ diameter of mirror in meters

$R = 1 \cdot 10^{-2}$ radius of curvature of mirror in meters

$$\Delta = R - \sqrt{R^2 - \left(\frac{\Phi}{2}\right)^2}$$ difference between center thickness of mirror and edge thickness.

$t_e = 4 \cdot 10^{-3}$ edge thickness of mirror

$t_c = t_e - \Delta$ $t_c = 3.218697 \cdot 10^{-3}$ center thickness of mirror

Matrix for mirror

$$\begin{pmatrix} A' & B' \\ C' & D' \end{pmatrix} = \begin{bmatrix} 1 & \dfrac{t_c}{n} \\ \dfrac{1-n}{(-R)} & \dfrac{1-n}{(-R)} \cdot \dfrac{t_c}{n} - 1 \end{bmatrix}$$ (-R) due to sign convention.

<u>Input Pump Beam parameters</u>:

$w_0 = 19 \cdot 10^{-6}$ $\lambda = 979.7 \cdot 10^{-9}$

$$z_{R1} = \frac{\pi \cdot w_0^2}{\lambda}$$ $z_{R1} = 1.158 \cdot 10^{-3}$

<u>Beam Transformation (waist to waist)</u>:
$A(s3) = A' + C' \cdot s3$ $B(s1, s3) = A' \cdot s1 - C' \cdot s1 \cdot s3 - B' - D' \cdot s3$

$C = C'$ $D(s1) = C' \cdot s1 + D'$

<u>Waist Location of Transformed Beam</u>:
$$s3(s1) = -\frac{A' \cdot C' \cdot z_{R1}^2 + (A' \cdot D' + B' \cdot C') \cdot s1 + A' \cdot C' \cdot s1^2 + B' \cdot D'}{C'^2 \cdot z_{R1}^2 - C'^2 \cdot s1^2 + 2 \cdot C' \cdot D' \cdot s1 + D'^2}$$

<u>Waist Size of Transformed Pump Beam</u>:
$$w0_p(s1, s3) = \frac{\lambda}{\pi} \cdot \left[\frac{(A(s3) \cdot D(s1) - B(s1, s3) \cdot C) \cdot z_{R1}}{D(s1)^2 - C^2 \cdot z_{R1}^2}\right]^{0.5}$$
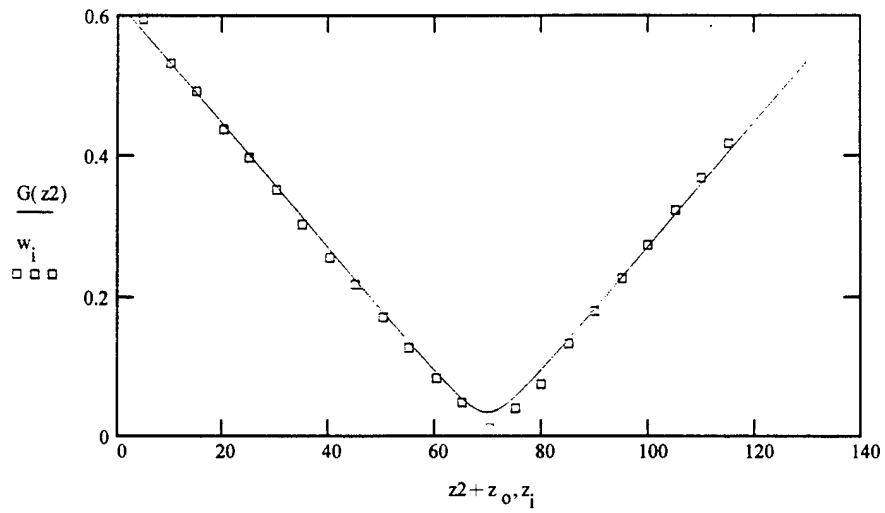
<u>Waist Size of Cavity Mode</u>:
$$g(s) = 1 - \frac{2 \cdot s}{R} \qquad w0_c(s) = \left[\frac{s \cdot \lambda}{\pi} \cdot \sqrt{\frac{1 - g(s)}{1 - g(s)}}\right]^{0.5}$$

51

Plot of data and best curve line.

$$G(z2) = w_o \cdot \sqrt{1 + \left[\frac{\lambda \cdot (z2)}{\pi \cdot w_o^2}\right]^2} \qquad z2 = -75, -74 .. 60 \qquad i = 0 .. 22$$

This program calculates the mirror positions for the degenerate OPO cavity with the MOPA diode laser.

<u>Input Cavity Mirror:</u> $TOL \equiv 10^{-6}$

$n = 1.4507$ index of refraction of mirror

$\Phi = 7.75 \cdot 10^{-3}$ diameter of mirror in meters

$R = 1 \cdot 10^{-2}$ radius of curvature of mirror in meters

$\Delta = R - \sqrt{R^2 - \left(\dfrac{\Phi}{2}\right)^2}$ difference between center thickness of mirror and edge thickness.

$t_e = 4 \cdot 10^{-3}$ edge thickness of mirror

$t_c = t_e - \Delta \quad t_c = 3.218697 \cdot 10^{-3}$ center thickness of mirror

Matrix for mirror

$$\begin{pmatrix} A' & B' \\ C' & D' \end{pmatrix} := \begin{bmatrix} 1 & \dfrac{t_c}{n} \\ \dfrac{1-n}{(-R)} & \dfrac{1-n}{(-R)} \cdot \dfrac{t_c}{n} + 1 \end{bmatrix}$$

(-R) due to sign convention.

<u>Input Pump Beam parameters</u>:

$w_o = 19 \cdot 10^{-6} \qquad \lambda := 979.7 \cdot 10^{-9}$

$z_{R1} = \dfrac{\pi \cdot w_o^2}{\lambda} \qquad z_{R1} = 1.158 \cdot 10^{-3}$

<u>Beam Transformation (waist to waist)</u>:

$A(s3) = A' + C' \cdot s3$ $B(s1,s3) = A' \cdot s1 + C' \cdot s1 \cdot s3 + B' + D' \cdot s3$

$C = C'$ $D(s1) = C' \cdot s1 + D'$

<u>Waist Location of Transformed Beam</u>:

$$s3(s1) = -\dfrac{A' \cdot C' \cdot z_{R1}^2 + (A' \cdot D' + B' \cdot C') \cdot s1 + A' \cdot C' \cdot s1^2 + B' \cdot D'}{C'^2 \cdot z_{R1}^2 + C'^2 \cdot s1^2 + 2 \cdot C' \cdot D' \cdot s1 + D'^2}$$

<u>Waist Size of Transformed Pump Beam</u>:

$$w0_p(s1,s3) = \left[\dfrac{\lambda}{\pi} \cdot \dfrac{(A(s3) \cdot D(s1) - B(s1,s3) \cdot C) \cdot z_{R1}}{D(s1)^2 - C^2 \cdot z_{R1}^2}\right]^{0.5}$$
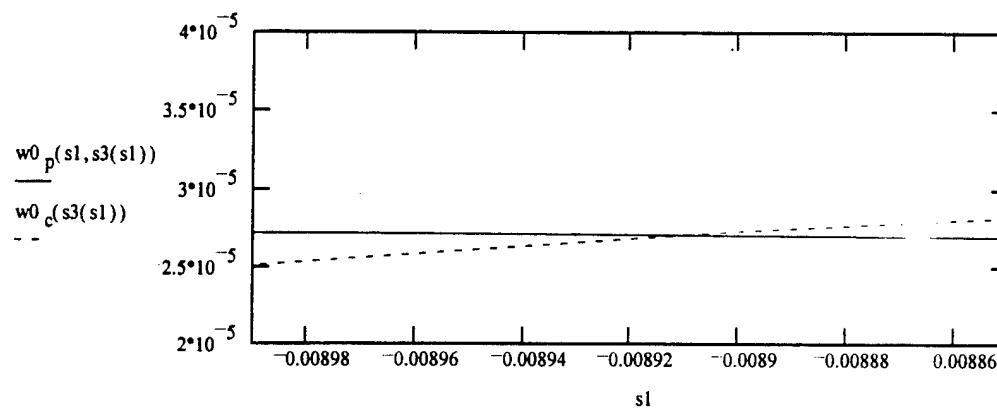
<u>Waist Size of Cavity Mode</u>:

$$g(s) = 1 - \dfrac{2 \cdot s}{R} \qquad w0_c(s) = \left[\dfrac{s \cdot \lambda}{\pi} \cdot \dfrac{1 - g(s)}{1 - g(s)}\right]^{0.5}$$

Position of Mirror from Input Beam Waist
(neg means mirror is before the waist):

$$s1 := -9 \cdot 10^{-3}, -8.9 \cdot 10^{-3} .. \; 7.0 \cdot 10^{-3}$$

$$\frac{w0_p(s1, s3(s1))}{w0_c(s3(s1))}$$

- -

Match Waist Sizes at same position after the mirror:

$$s1 := -9 \cdot 10^{-3}$$

GIVEN $\quad w0_c(s3(s1)) = w0_p(s1, s3(s1)) \qquad S1 := \text{find}(s1) \qquad S1 = -8.91 \cdot 10^{-3}$

$S3 := s3(S1) \qquad S3 = 9.41 \cdot 10^{-3} \qquad w0_c(S3) = 2.713 \cdot 10^{-5} \qquad w0_p(S1, S3) = 2.713 \cdot 10^{-5}$

This program calculates the beam waist radius for measured data.

Experimental steps:

1. Measure the beam using a scanning razor blade at the $1/e^2$ points - 86% and 14%. Do this for both the horizontal and vertical directions.

2. Plot the data and determine to a best approximation where the beam waist is.

$$TOL = 10^{-6}$$

Set up matrices for the measured beam data. z = distance from front of mirrormount point, w = beam radius

These are in units of millimeters.

$z = (5 \quad 10 \quad 15 \quad 20 \quad 25 \quad 30 \quad 35 \quad 40 \quad 45 \quad 50 \quad 55 \quad 60 \quad 65 \quad 70 \quad 75 \quad 80 \quad 85 \quad 90 \quad 95 \quad 100 \quad 105 \quad 110 \quad 115)^T$

$w = (.595 \quad .53 \quad .49 \quad .435 \quad .395 \quad .35 \quad .3 \quad .255 \quad .215 \quad .17 \quad .1275 \quad .0825 \quad .0495 \quad .0118 \quad .0395 \quad .0743 \quad .1325 \quad .1$

Given data: $\lambda = 979.5 \cdot 10^{-6}$ $z_o = 69.75$

Sample guess value for solve block: $w_o = 0.030$

Equation for gaussian beam profile:

$$f(z, z_o, w_o) = w_o \cdot \sqrt{1 + \left[\frac{\lambda \cdot (z - z_o)}{\pi \cdot w_o^2} \right]^2}$$
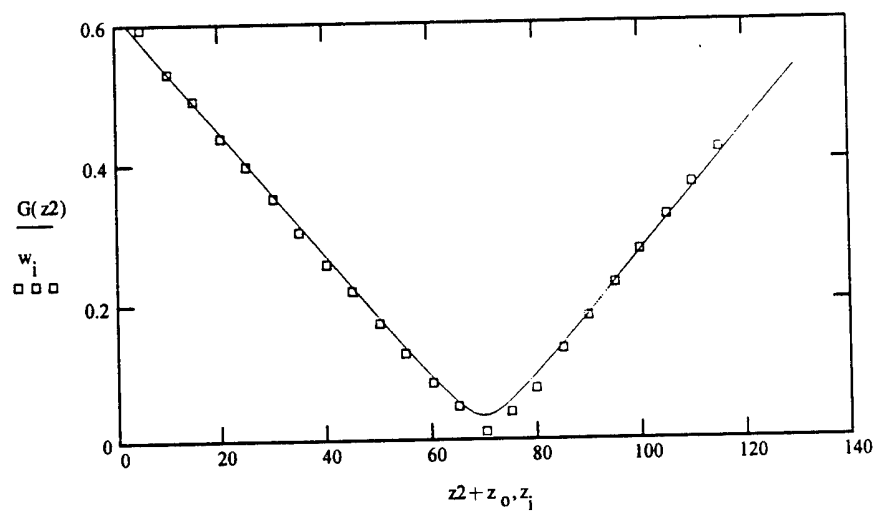
Solve block for minerr function.
Given

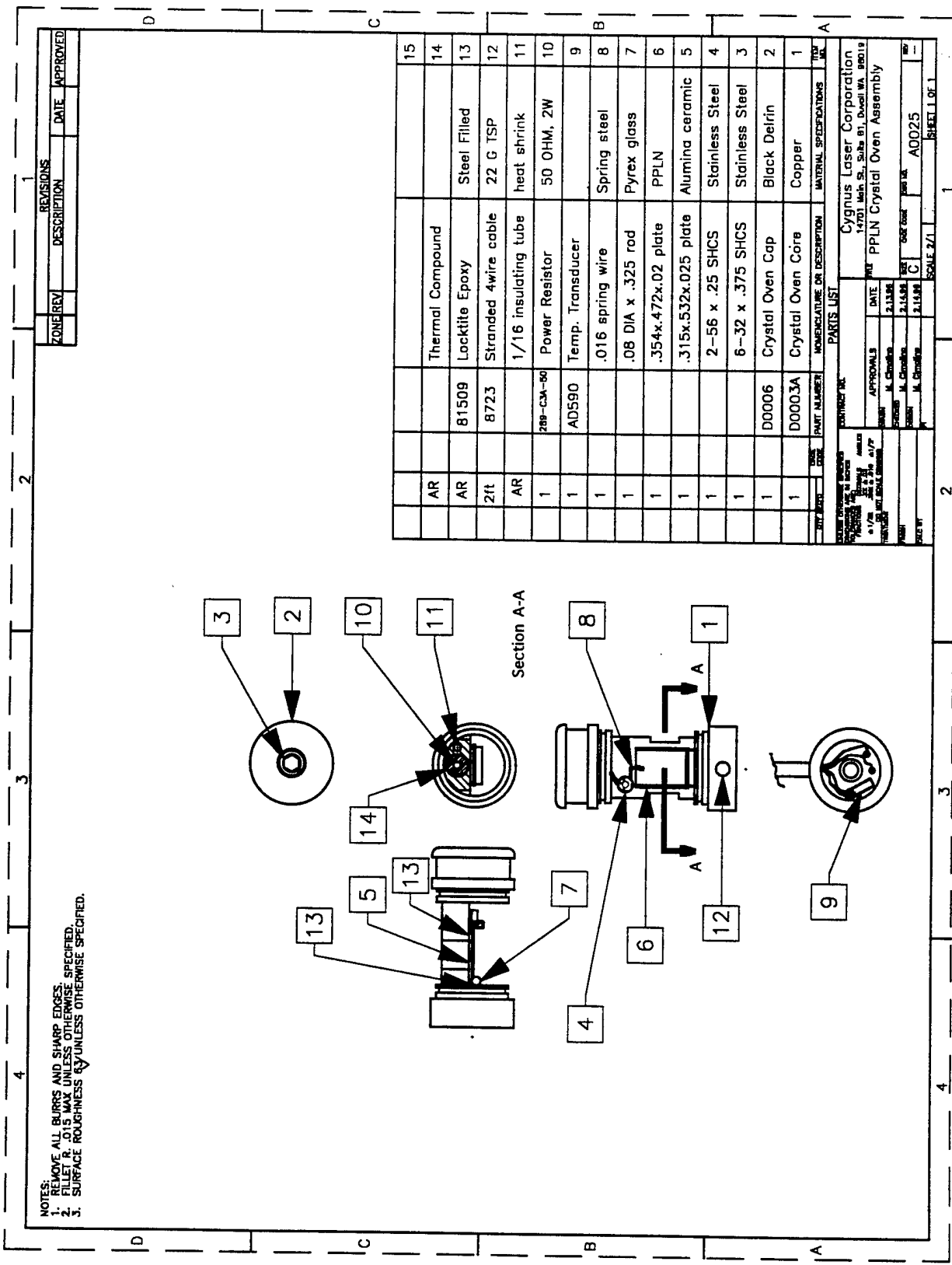$$\left| \vec{w} - \overline{f(z, z_o, w_o)} \right| = 0 \qquad w_o > 0 \qquad w_o = minerr(w_o) \qquad w_o = 0.035$$

Plot of data and best curve line.

$$G(z2) = w_0 \cdot \sqrt{1 + \left[\frac{\lambda \cdot (z2)}{\pi \cdot w_0^2}\right]^2} \qquad z2 = -75, -74 .. 60 \qquad i = 0 .. 22$$
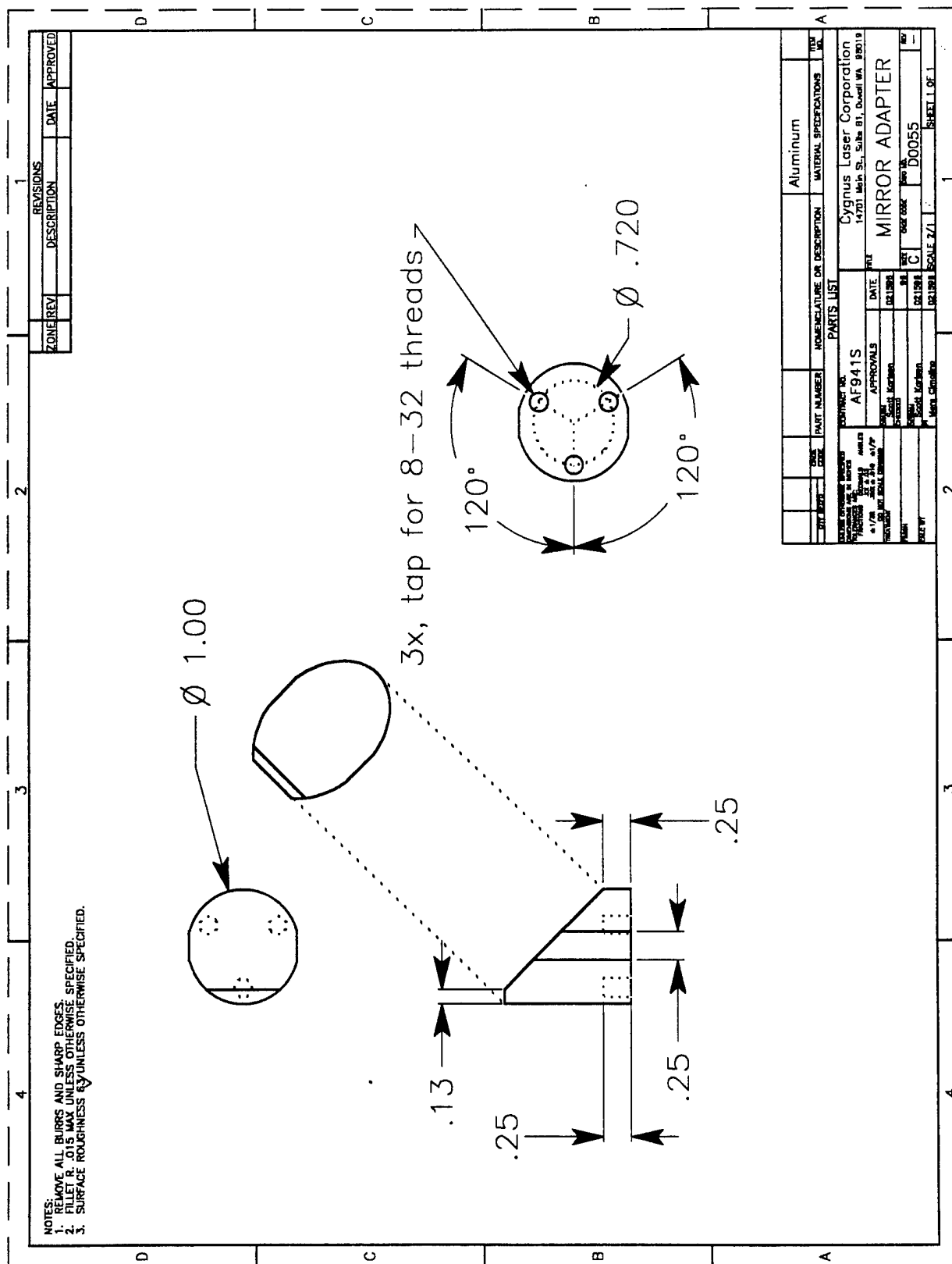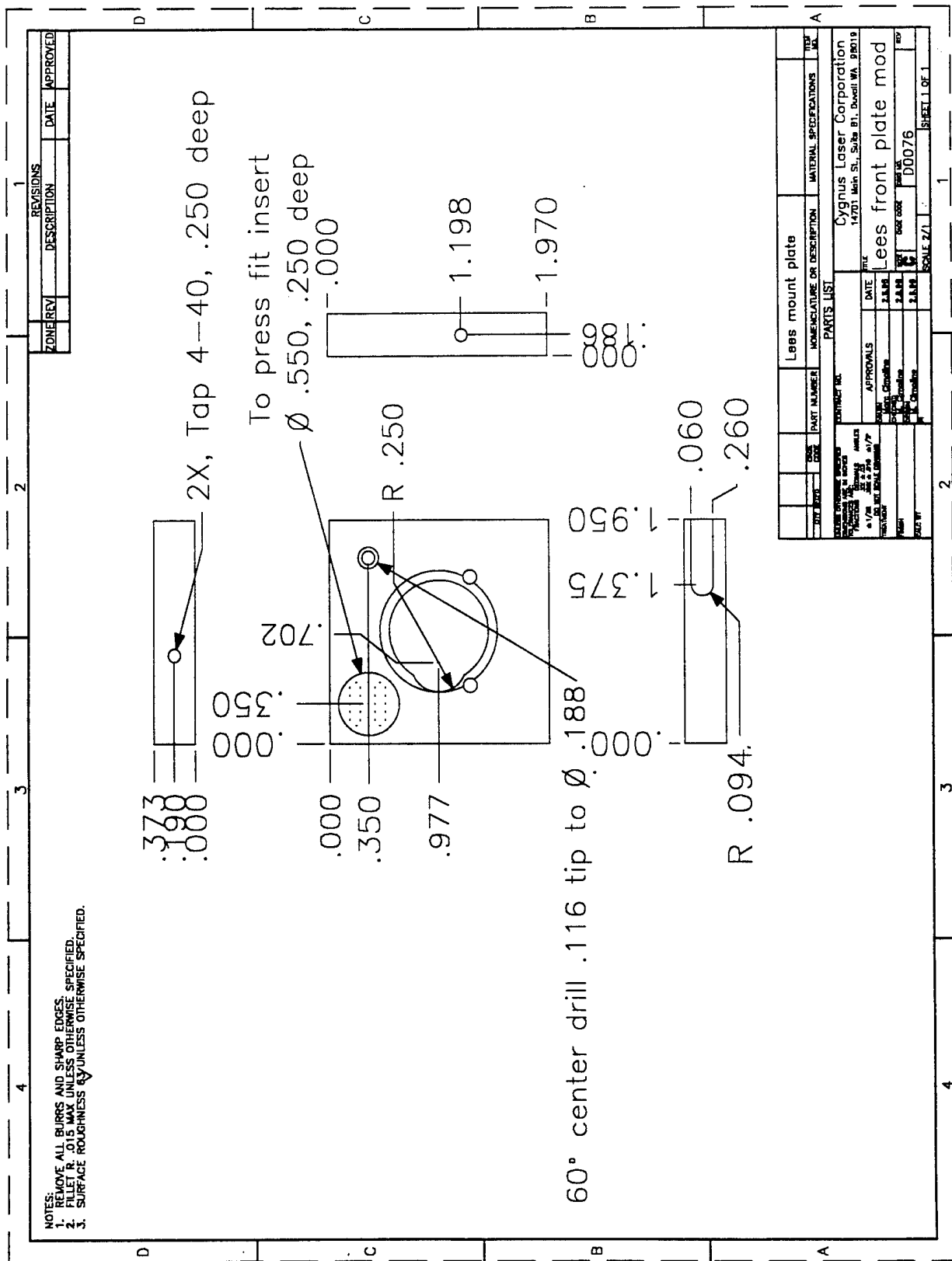
C APPENDIX C
MECHANICAL DRAWINGS

NOTES:
1. REMOVE ALL BURRS AND SHARP EDGES.
2. FILLET R .015 MAX UNLESS OTHERWISE SPECIFIED.
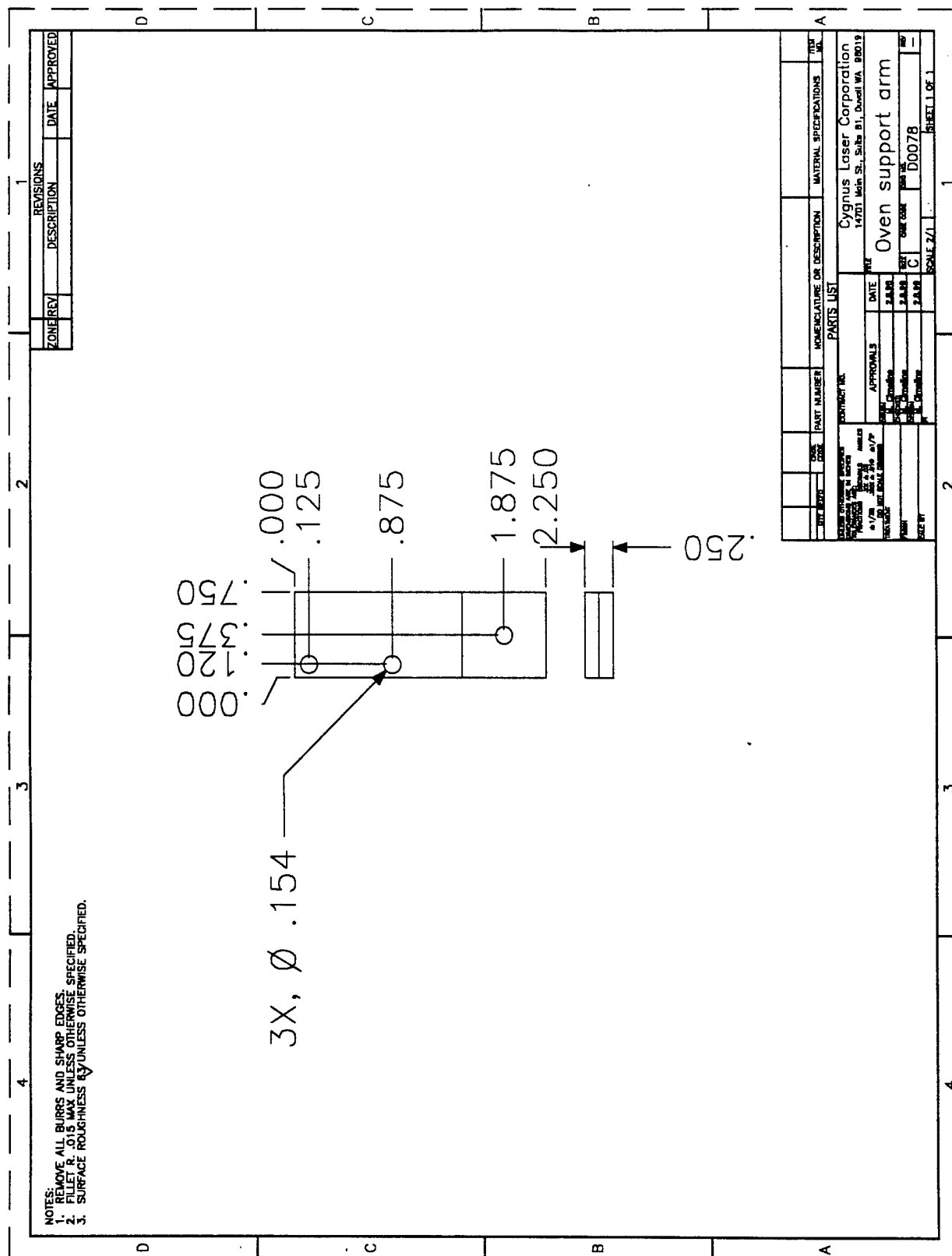3. SURFACE ROUGHNESS 63 UNLESS OTHERWISE SPECIFIED.

Ø .064 THRU
Ø .75
Ø .65
Ø .551

1.251
1.18
1.126
.778
.515
.376

.456

.304

.25

0

Section A-A

.027

.125

064 THRU, C'BORE Ø .204 DEPTH .70

REVISIONS
ZONE | REV | DESCRIPTION | DATE | APPROVED

Copper | Cu:Te Alloy

Cygnus Laser Corporation
14701 Main St., Suite B1, Duvall WA 98019

Crystal Oven Core

D0003

SHEET 1 OF 1
SCALE 2/1

PARTS LIST
ITEM NO. | PART NUMBER | NOMENCLATURE OR DESCRIPTION | MATERIAL SPECIFICATIONS
1

APPROVALS | DATE
DRAWN | M. Claredine
CHECKED | M. Claredine
ISSUED | M. Claredine

Section A-A

ITEM NO	QTY	PART NUMBER	NOMENCLATURE OR DESCRIPTION	MATERIAL SPECIFICATIONS
15				
14	AR		Thermal Compound	
13	AR	81509	Locktite Epoxy	Steel Filled
12	2ft	8723	Stranded 4wire cable	22 G TSP
11	AR		1/16 insulating tube	heat shrink
10	1	289-C3A-50	Power Resistor	50 OHM, 2W
9	1	AD590	Temp. Transducer	
8	1		.016 spring wire	Spring steel
7	1		.08 DIA x .325 rod	Pyrex glass
6	1		.354x.472x.02 plate	PPLN
5	1		.315x.532x.025 plate	Alumina ceramic
4	1		2-56 x .25 SHCS	Stainless Steel
3	1		6-32 x .375 SHCS	Stainless Steel
2	1	D0006	Crystal Oven Cap	Black Delrin
1	1	D0003A	Crystal Oven Core	Copper

PARTS LIST

Cygnus Laser Corporation
14701 Main St., Suite 81, Duvall WA 98019

TITLE: PPLN Crystal Oven Assembly

	APPROVALS	DATE
DRAWN	M. Cirsatino	2.11.94
CHECKED	M. Cirsatino	2.11.94
DESIGN	M. Cirsatino	2.11.94

SIZE: C DWG NO: A0025 REV: –

SCALE 2/1 SHEET 1 OF 1

REVISIONS

ZONE	REV	DESCRIPTION	DATE	APPROVED

slot .375 long x .272

Ø .272

.75

.25

.00

.88

.375

.19

.00

relieve 0.01"

.25

.25

2x, drill and tap
for 1-72 threads

.20

.10

.88

.625

.13

.00

1.13

.59

.00

REVISIONS

ZONE	REV	DESCRIPTION	DATE	APPROVED
D4	1	change hole to slot	052998	

Aluminum

MATERIAL SPECIFICATIONS

Cygnus Laser Corporation
14701 Main St., Suite B1, Dovell MA 95019

LOW OVEN MOUNT

DWG NO. D0051   REV A

SHEET 1 OF 1

SCALE 3/1

PARTS LIST

NOMENCLATURE OR DESCRIPTION

PART NUMBER
AF941S

APPROVALS   DATE

SIZE C

PART NO. M4

012398

NOTES:
1. REMOVE ALL BURRS AND SHARP EDGES.
2. FILLET R .015 MAX UNLESS OTHERWISE SPECIFIED.
3. SURFACE ROUGHNESS 63 UNLESS OTHERWISE SPECIFIED.

relieve .010"

tap for 4-40

Ø .154

1.00
.63
.13
.00

.75
.58
.45
.15
.00

.089

.25
.10
.25

counterbore for 1-72
socket head cap screw

1.25
.72
.59
.27
.14
.00

1.00
.63
.00
.140

REVISIONS
ZONE | REV | DESCRIPTION | DATE | APPROVED

Aluminum

MATERIAL SPECIFICATIONS

NOMENCLATURE OR DESCRIPTION

PARTS LIST

PART NUMBER | ITEM NO.

CONTRACT NO.
AF941S

APPROVALS

Cygnus Laser Corporation
14701 Main St., Suite 81, Duvall WA 98019

TOP OVEN MOUNT

D0052

SHEET 1 OF 1

SCALE 3/1

NOTES:
1. REMOVE ALL BURRS AND SHARP EDGES.
2. FILLET R .015 MAX UNLESS OTHERWISE SPECIFIED.
3. SURFACE ROUGHNESS 63 UNLESS OTHERWISE SPECIFIED.

4x, drill and tap for 4-40 thread

8x, drill and tap
for 8-32 thread

Aluminum

MATERIAL SPECIFICATIONS

NOMENCLATURE OR DESCRIPTION

PARTS LIST

Cygnus Laser Corporation
14701 Main St., Suite 81, Dowell MA. 98019

U-BEAM FOR DIODE PUMPED
OPO BOX

PART NUMBER
AF841S

D0053

SHEET 1 OF 1

MOPA CLAMP — Cygnus Laser Corporation

NOTES:
1. REMOVE ALL BURRS AND SHARP EDGES.
2. FILLET R. .015 MAX UNLESS OTHERWISE SPECIFIED.
3. SURFACE ROUGHNESS UNLESS OTHERWISE SPECIFIED.

Ø .272

.75

.57

.050

1.03

.5

.75

2x, press fit to .23 dowel pin

.38

2.00

1.00

.750

chamfer edges

REVISIONS
ZONE | REV | DESCRIPTION | DATE | APPROVED

PARTS LIST
ITEM NO. | PART NUMBER | NOMENCLATURE OR DESCRIPTION | MATERIAL SPECIFICATIONS

Aluminum

Cygnus Laser Corporation
14701 Main St., Suite B1, Duvall WA 98019

TITLE: MOPA CLAMP

CONTRACT NO.
PART NUMBER AF941S

DWG NO. D0054

SIZE C   CAGE CODE   REV —

SHEET 1 OF 1

SCALE 2/1

Ø .720

Ø 1.00

3x, tap for 8-32 threads

120°

120°

.25

.13

.25

.25

REVISIONS
ZONE | REV | DESCRIPTION | DATE | APPROVED

Aluminum
MATERIAL SPECIFICATIONS

NOMENCLATURE OR DESCRIPTION
PARTS LIST

Cygnus Laser Corporation
14701 Main St., Suite B1, Duvall WA 98019

MIRROR ADAPTER

CONTRACT NO.
PART NUMBER
AF941S

APPROVALS
DRAWN | Scott Karlsen | DATE | 021591
CHECKED
DESIGN | Scott Karlsen | 021591
| Mark Cimolino

SIZE | CAGE CODE | DWG NO.
C | | D0055

REV
C

SCALE 2/1 | SHEET 1 OF 1

2x, Through hole for 1/4-20
socket head cap screw

Countersink for 1/4-20
socket head cap screw

3.07

2.571

1.54

.25

.00

.00

.75

1.50

.668

REVISIONS

ZONE	REV	DESCRIPTION	DATE	APPROVED

Aluminum

Cygnus Laser Corporation
14701 Main St., Suite B1, Duvall WA 98019

NOMENCLATURE OR DESCRIPTION   MATERIAL SPECIFICATIONS

PARTS LIST

PART NUMBER

CONTRACT NO.
AF941S

TITLE
Isolator Riser Two

APPROVALS   DATE

DRAWN   Scott Karlsen   021991

CHECKED

Scott Karlsen   021991

Merv Chaulke   021991

CAGE CODE   DWG NO.
C   D0061

REV

SCALE 2/1   SHEET 1 OF 1

NOTES:
1. REMOVE ALL BURRS AND SHARP EDGES.
2. FILLET R. .015 MAX UNLESS OTHERWISE SPECIFIED.
3. SURFACE ROUGHNESS 63/UNLESS OTHERWISE SPECIFIED.

2x, R .125

45°

4.053

1.250
.875
.125
.000

4x, counterbore
for 8-32 thread

45°
.063

8.105

3.500

1.813

4x, .375

7.605

.250

6.188
5.776
.063

.376

1.625

.000

.063

4x, drill and tap
for 8-32 thread

.375

.000
.375

4.375

.375
.156

Press fit stainless steel washer
for 1/4-20 screw to protrude

Aluminum

MATERIAL SPECIFICATIONS

NOMENCLATURE OR DESCRIPTION

PARTS LIST

PART NUMBER
AF941S

Cygnus Laser Corporation
14701 Main St., Suite 81, Duvall WA 98019

TITLE
REAR END PLATE FOR
DIODE PUMPED OPO

DWG NO.
D0066

SHEET 1 OF 1

REVISIONS
ZONE | REV | DESCRIPTION | DATE | APPROVED

APPROVALS | DATE
Scott Karlsen
Scott Karlsen
Nora Chuahin

SCALE 1/3

NOTES:
1. REMOVE ALL BURRS AND SHARP EDGES.
2. FILLET R. .015 MAX UNLESS OTHERWISE SPECIFIED.
3. SURFACE ROUGHNESS 63 UNLESS OTHERWISE SPECIFIED.

2X, Tap 4-40, .250 deep

To press fit insert
Ø .550, .250 deep

R .250

60° center drill .116 tip to Ø.188

R .094

1.198
1.970
1.950
1.375
.977
.702
.350
.000
.260
.060
.000
.188
.100
.000
.373
.198
.088
.350
.000

REVISIONS
ZONE | REV | DESCRIPTION | DATE | APPROVED

Lees mount plate
PART NUMBER | NOMENCLATURE OR DESCRIPTION | MATERIAL SPECIFICATIONS | ITEM NO.
PARTS LIST

Cygnus Laser Corporation
14701 Main St., Suite B1, Duvall WA 98019

Lees front plate mod

DWG NO. D0076

SHEET 1 OF 1

NOTES:
1. REMOVE ALL BURRS AND SHARP EDGES.
2. FILLET R .015 MAX UNLESS OTHERWISE SPECIFIED.
3. SURFACE ROUGHNESS 63 UNLESS OTHERWISE SPECIFIED.

3X, Ø .154

.000
.125
.875
1.875
2.250

.250

.750
.375
.120
.000

REVISIONS
ZONE | REV | DESCRIPTION | DATE | APPROVED

PARTS LIST
ITEM NO. | PART NUMBER | NOMENCLATURE OR DESCRIPTION | MATERIAL SPECIFICATIONS

Cygnus Laser Corporation
14701 Main St., Suite B1, Duvall WA 98019

Oven support arm

CAGE CODE | DWG NO. D0078 | REV

SCALE 2/1 | SHEET 1 OF 1

APPROVALS

69

piezo mount

Cygnus Laser Corporation
14701 Main St., Suite 81, Duvall WA. 98019

NOMENCLATURE OR DESCRIPTION
PART NUMBER
CONTRACT NO.
PARTS LIST
MATERIAL SPECIFICATIONS

DWG NO. D0079
SCALE 4/1
SHEET 1 OF 1

.590
.090
.000

.304
3X, TAP 4-40 thru
Ø .154 THRU
.369
.238
.138
135.00° .163
.309
.238
2X, .304
Ø .393 THRU
Ø .885
Ø 1.050

REVISIONS
ZONE | REV | DESCRIPTION | DATE | APPROVED

NOTES:
1. REMOVE ALL BURRS AND SHARP EDGES.
2. FILLET R. .015 MAX UNLESS OTHERWISE SPECIFIED.
3. SURFACE ROUGHNESS 63 UNLESS OTHERWISE SPECIFIED.

Ø .125

Ø .393

Ø .768

Piezo end cap

.160

Cable Clamp

NOTES:
1. REMOVE ALL BURRS AND SHARP EDGES.
2. FILLET R. .015 MAX UNLESS OTHERWISE SPECIFIED.
3. SURFACE ROUGHNESS 63 UNLESS OTHERWISE SPECIFIED.

REVISIONS
ZONE | REV | DESCRIPTION | DATE | APPROVED

Stainless Steel

PART NUMBER | NOMENCLATURE OR DESCRIPTION | MATERIAL SPECIFICATIONS | ITEM NO.
PARTS LIST

Cygnus Laser Corporation
14701 Main St., Suite B1, Duvall WA 98019

Piezo End Cap

D0084

SHEET 1 OF 1

SCALE 2/1

NOTES:
1. REMOVE ALL BURRS AND SHARP EDGES.
2. FILLET R .015 MAX UNLESS OTHERWISE SPECIFIED.
3. SURFACE ROUGHNESS UNLESS OTHERWISE SPECIFIED.

REVISIONS

ZONE	REV	DESCRIPTION	DATE	APPROVED
C3	1	add notch in vent hole	052996	
C3	2	add Ø.067 slot	052996	
C3	3	add Ø.159 slot	052996	

.130

4x, drill and tap for
4-40 thread

slot .159 wide

slot .067 wide

.375

3.542
3.168
2.943

2.500

2.523
2.323

1.500
1.313
1.143

.918

2x, R .125

slot .375 wide

.793
.543
.000

5.750
5.675

4.875
4.625

.625

.000

Cygnus Laser Corporation
14701 Main St., Suite B1, Duvall WA. 980119

VENT DETAIL

PART NUMBER
AF941S

PARTS LIST

NOMENCLATURE OR DESCRIPTION   MATERIAL SPECIFICATIONS

DWG NO. D0104

SHEET 1 OF 1

72

EXHAUST VENT COVER

Cygnus Laser Corporation
14701 Main St., Suite 81, Duvall WA. 980109

PART NUMBER: AF941S

Aluminum

PARTS LIST

MATERIAL SPECIFICATIONS

DWG NO. D0105

SHEET 1 OF 1

NOTES:
1. REMOVE ALL BURRS AND SHARP EDGES.
2. FILLET R. .015 MAX UNLESS OTHERWISE SPECIFIED.
3. SURFACE ROUGHNESS 63√UNLESS OTHERWISE SPECIFIED.

REVISIONS

ZONE	REV	DESCRIPTION	DATE	APPROVED
B3	3	add Ø.087 round notch	052996	
B3	2	add Ø.159 round notch	052996	
B2	1	add countersink	052996	

4x, Ø .112

8x, R .250

4x, c/sink to fit 4-40 flathead screw

3.000

2.656
2.625

1.980

1.780

1.500

R .080

R .034

R .188

2.500

.375

.344

.250

.000

.625

.250

.000

1.125

.125

.040

NOTES:
1. REMOVE ALL BURRS AND SHARP EDGES.
2. FILLET R. .015 MAX UNLESS OTHERWISE SPECIFIED.
3. SURFACE ROUGHNESS 63 √ UNLESS OTHERWISE SPECIFIED.

.000
1.500 ±.001
2.000 ±.001
2.500 ±.001
3.125 ±.002
3.625 ±.002
4.715 ±.002
4.750 ±.002
5.500 ±.001
6.000 ±.001
6.500 ±.001
7.250 ±.002
7.285 ±.002
8.000

24.500
21.988 ±.01
16.740 ±.01
13.286 ±.01
13.116 ±.01
7.286 ±.001
7.222 ±.001
4.630 ±.001
4.116 ±.01
2.552 ±.005
.000

Ø .252 ±.001
Ø .252 ±.001
2x, Ø .252 ±.001
10x, Ø .272
8x, drill and tap for 1/4-20 thread

Cygnus Laser Corporation
14701 Main St., Suite B1, Duvall WA. 98019

DIODE PUMPED OPO MOUNTING
HOLE PATTERN

PARTS LIST
PART NUMBER
AF941S

D0106
SHEET 1 OF 1

DISTRIBUTION LIST

AUL/LSE
Bldg 1405 - 600 Chennault Circle
Maxwell AFB, AL 36112-6424   1 cy

DTIC/OCP
8725 John J. Kingman Rd, Suite 0944
Ft Belvoir, VA 22060-6218   2 cys

AFSAA/SAI
1580 Air Force Pentagon
Washington, DC 20330-1580   1 cy

PL/SUL
Kirtland AFB, NM 87117-5776   2 cys

PL/HO
Kirtland AFB, NM 87117-5776   1 cy

Official Record Copy
PL/LIDA/Shaw   2 cys

Cynus Laser Corporation
P.O. BOX 1730
Duvall, WA 98019-1730   1 cy